

# Impact of operation parameters and lambda input signal during lambda-dithering of three-way catalysts for low-temperature performance enhancement

Daniel Hodonj<sup>a</sup>, Michael Borchers<sup>a</sup>, Lukas Zeh<sup>a</sup>, Gia Trung Hoang<sup>a</sup>, Steffen Tischer<sup>b</sup>, Patrick Lott<sup>a,\*</sup>, Olaf Deutschmann<sup>a,b</sup>

<sup>a</sup> Institute for Chemical Technology and Polymer Chemistry (ITCP), Karlsruhe Institute of Technology (KIT), Engesserstr. 20, 76131 Karlsruhe, Germany

<sup>b</sup> Institute of Catalysis Research and Technology (IKFT), Karlsruhe Institute of Technology (KIT), Hermann-von-Helmholtz-Platz 1, 76344 Eggenstein-Leopoldshafen, Germany

## ARTICLE INFO

### Keywords:

Dithering  
Oxygen storage capacity  
Palladium  
Periodic operation  
Three-way catalyst

## ABSTRACT

A synthetic exhaust gas bench was dynamically operated to investigate the impact of temperature, amplitude, split cycle, mean lambda, gas hourly space velocity, and oxygen storage capacity on average pollutant conversion and product selectivity of three-way catalysts in periodic operation. As temperature and amplitude increase and oxygen storage capacity decreases, the optimal frequency for maximum pollutant conversion increases. This is consistent with faster desorption of CO and O<sub>2</sub> from the catalyst, yielding free surface sites. Regarding the formation of secondary products, the optimal frequency for maximum pollutant conversion does not always correspond to minimal N<sub>2</sub>O and NH<sub>3</sub> emissions. The split cycle variation reveals the enhancement of C<sub>3</sub>H<sub>8</sub> and NO conversion after both lean-rich and rich-lean switches and C<sub>3</sub>H<sub>6</sub> and CO conversion after rich-lean switches at the optimal frequency. As periodic operation does not affect existing engine settings or operating conditions, it is a cost-effective control strategy for meeting future emission limits.

## 1. Introduction

Compared to conventional internal combustion engines (ICE), modern hybrid electric vehicles (HEV) can save up to 49% fuel under urban driving conditions, which results in lower carbon dioxide (CO<sub>2</sub>) emissions [1]. However, frequent stops and restarts of the HEV engine are accompanied by periods of low exhaust temperatures and therefore lead to a decrease in pollutant conversion in the three-way catalyst (TWC), which is used as the exhaust gas aftertreatment system to abate carbon monoxide (CO), nitrogen oxides (NO<sub>x</sub>), and unburned hydrocarbons (HC). Once the Euro 7 standards [2] come into force, new challenges arise for the exhaust gas aftertreatment of ICEs [3]. In addition to reliable pollutant conversion at low exhaust temperatures, legislation also calls for the reduction of secondary emissions such as N<sub>2</sub>O and NH<sub>3</sub> and doubles the requirement for the service life of exhaust gas aftertreatment systems from 100 000 km and 5 years to 200 000 km and 10 years.

To allow simultaneous conversion of CO, NO<sub>x</sub> and HC, gasoline engines equipped with a TWC are usually operated in a narrow range of

air-fuel equivalence ratio (AFR) at  $\lambda = 1$ . In comparison to a continuous stoichiometric operation, forced periodic switches between a lean and rich exhaust gas, known as lambda-dithering, has been reported to increase the pollutant conversion of the TWC under particular conditions [4–7,8,9]. Especially the frequency, which describes how fast the period of the lean and rich half-cycle is repeated, influences the pollutant conversion over the catalyst. Toyota scientists systematically investigated the effect of frequency on the performance of Pt, Pd and Rh-based TWCs for CO oxidation [10], C<sub>3</sub>H<sub>6</sub> oxidation [11], NO reduction with CO [12], and with synthetic exhaust gas [5]. They observed a narrow band of dithering frequency that increases the conversion for each reaction above the value reached at constant stoichiometric operation. The band can be characterized by the critical or optimum frequency [4]. The origin of the rate increase due to periodic operation has not yet been conclusively clarified. It is assumed that the reaction under stoichiometric, lean and rich steady-state conditions is hindered by the occupancy of the catalyst by the most strongly adsorbing species in each particular case [13–15]. For instance, surface blockage by adsorbed O-atoms was reported as primary obstacle for high pollutant conversion under lean conditions [16]. By selecting a suitable fluctuating operating

\* Corresponding author.

E-mail address: [patrick.lott@kit.edu](mailto:patrick.lott@kit.edu) (P. Lott).

<https://doi.org/10.1016/j.apcatb.2023.123657>

**Nomenclature***Greek symbols*

$\lambda$	Air-fuel equivalence ratio (-)
$\lambda_m$	Mean lambda (-)
$\lambda_\phi$	Time-averaged lambda (-)
$\nu_i$	Stoichiometric coefficient of species $i$ (-)
$\tau$	Cycle period (s)
$\tau_L$	Lean cycle period (s)

*Latin symbols*

$A$	Amplitude (-)
$A_{\text{real}}$	Real amplitude (-)
$D_{\text{Pd}}$	Dispersion of Pd (-)
$f$	Frequency (Hz)
$GHSV$	Gas hourly space velocity ( $\text{h}^{-1}$ )

$m_{\text{cat}}$	Mass of catalyst (g)
$M_{\text{Pd}}$	Molar mass of Pd ( $\text{g mol}^{-1}$ )
$n\tau$	Multiple of the cycle period (s)
$p$	Pressure (Pa)
$s_L$	Split cycle (-)
$S_{i,\text{NO}}$	Selectivity of product $i$ derived from NO (-)
$t$	Time (s)
$T$	Temperature ( $^{\circ}\text{C}/\text{K}$ )
$TOF_i$	Turnover frequency of species $i$ ( $\text{s}^{-1}$ )
$v$	Velocity at 298 K ( $\text{m s}^{-1}$ )
$\dot{V}$	Flow rate ( $\text{m}^3 \text{s}^{-1}$ )
$X_i$	Time-averaged conversion of species $i$ (-)
$x_{\text{Pd}}$	Mass fraction of Pd (-)
$\bar{x}_i$	Time-averaged mole fraction of species $i$ (-)

condition of the engine, the strongly adsorbed species are removed from the catalyst on a regular basis, so that the surface composition of the adsorbates is brought to an equal level, thus increasing the reaction rate [17] and reducing secondary emissions [18]. Notably, the use of dithering for emissions reduction does not interfere with existing engine settings or run conditions and does not require a complex feedback system. Therefore, it is a cost-effective emission control strategy to comply with future stricter emission limits [19,20].

However, due to the constantly changing operating conditions of an ICE, TWCs are generally subject to substantial fluctuations in terms of temperature and volume flow [21]. These conditions can significantly influence the optimal fluctuating operating conditions [17]. In addition, there are control variables such as the split cycle, which indicates the ratio between the lean cycle period and the cycle period, the amplitude, which describes the extent between lean and rich magnitude, and the mean lambda. All these parameters influence the catalyst performance during periodic operation to a relevant extent [20,22,23]. Furthermore, the use of support materials with oxygen storage properties can decisively influence the periodic operating conditions [24].

Therefore, the present study systematically investigates the influence of the catalyst operating conditions temperature and gas hourly space velocity ( $GHSV$ ), the influence of the control variables amplitude, split cycle, and mean lambda as well as the influence of oxygen storage material with respect to the optimum frequency for maximum pollutant conversion and minimum secondary emission selectivity in a laboratory test bench using synthetic exhaust gas.

## 2. Methodology

### 2.1. Catalyst preparation

For the preparation of the 2% Pd/ $\text{Al}_2\text{O}_3$  and the 2% Pd/ $\text{CeO}_2\text{-ZrO}_2$  (Pd/CZ) catalyst,  $\gamma\text{-Al}_2\text{O}_3$  (Puralox TH 100/150, Sasol) or CZ stabilized by a small amount of yttrium, neodymium and lanthanum dopants (Luxfer MEL Technologies) was calcined in static air for 5 h at 700  $^{\circ}\text{C}$ . Subsequently, Pd was added to the calcined supports by means of an incipient wetness impregnation (IWI). For this, an aqueous  $(\text{NH}_3)_4\text{Pd}(\text{NO}_3)_2$  solution (abcr) was used and the received powder was then dried for 4 h at 70  $^{\circ}\text{C}$  and calcined in air for 5 h at 500  $^{\circ}\text{C}$ . To examine the catalytic activity under realistic conditions, a cordierite monolith (3 cm length, 1.6 cm diameter, 400 cpsi, 4 mil, 97 cells; Corning) was coated with the catalyst powder. Analogous to the procedure applied by Karinshak et al. [25] the catalyst powder was mixed in a mass ratio of 90:10 with  $\text{AlO}(\text{OH})$  (Disperal P2, Sasol) and suspended in deionized water. After acidification with aqueous  $\text{HNO}_3$  (Fischer) the liquid slurry was added into the channels of a cordierite honeycomb by dip-coating.

Excess liquid was blown out before drying the monolith. This coating procedure was repeated until the desired catalyst loading of 100  $\text{g}_{\text{cat}} \text{L}^{-1}$  (approx. 57  $\text{g}_{\text{Pd}} \text{ft}^{-3}$ ) was reached and the monolith was calcined at 550  $^{\circ}\text{C}$  for 5 h. Prior to the catalytic activity tests, the samples were de-greened at the catalyst test bench with 10%  $\text{CO}_2$  and 10%  $\text{H}_2\text{O}$  ( $\text{N}_2$  balance) for 4 h at 600  $^{\circ}\text{C}$  at a  $GHSV$  of 50 000  $\text{h}^{-1}$ , analogous to the procedure proposed by Rappé et al. [26].

### 2.2. Catalyst characterization

$\text{N}_2$ -physisorption measurements were performed at a BELSORP-mini II (BEL Japan) after degassing the catalyst powders for 2 h at 300  $^{\circ}\text{C}$ . The obtained adsorption-desorption curves were evaluated using the method of Brunauer, Emmett, and Teller (BET) [27], which provides information on the specific surface area and pore volume. Inductively coupled plasma optical emission spectroscopy (ICP-OES) was used to validate the Pd loading of the powder catalysts. Temperature programmed reduction of the powder samples with hydrogen ( $\text{H}_2$ -TPR) was carried out in an AutoChem II (micromeritics). After an oxidative pretreatment (10%  $\text{O}_2$  in He, 10  $\text{K min}^{-1}$  to 500  $^{\circ}\text{C}$ ), the  $\text{H}_2$ -TPR was measured with 50  $\text{mL min}^{-1}$  of 10%  $\text{H}_2$  in Ar from -50 to 900  $^{\circ}\text{C}$  with 10  $\text{K min}^{-1}$ . A cryogenic cooler with liquid  $\text{N}_2$  allowed to reach low temperatures and a thermal conductivity detector (TCD) was used to detect the content of the effluent gas stream. High-angle annular dark-field scanning transmission electron microscopy (HAADF-STEM) combined with energy-dispersive X-ray spectroscopy (EDXS) was used to investigate the dispersion of Pd nanoparticles of the powder catalysts. The images were obtained at an FEI Osiris ChemiSTEM microscope at 200 keV electron energy, which is equipped with a Super-X EDXS system comprising four silicon drift detectors. To determine the particle size distribution, > 100 Pd nanoparticles were analyzed with the open source image processing software Fiji [28]. Analogous to earlier procedures applied in our group [29], Pd dispersion data of the monolithic samples were obtained by CO chemisorption measurements in a custom-made apparatus equipped with an IR detector (X-Stream, Emerson). The samples were oxidized in a quartz glass tubular reactor (Qsil) at 500  $^{\circ}\text{C}$  with atmospheric oxygen ( $\text{O}_2$ ) for 20 min and subsequently reduced at 400  $^{\circ}\text{C}$  for 60 min using 5% hydrogen ( $\text{H}_2$ ) in nitrogen ( $\text{N}_2$ ). After the reactor was cooled to room temperature under  $\text{N}_2$  flushing the catalyst was saturated with 1% CO in  $\text{N}_2$ . Gaseous and physisorbed CO are then flushed away via a nitrogen stream before the temperature-programmed desorption of the CO takes place under inert nitrogen flow during heating with a rate of 20  $\text{K min}^{-1}$  to 550  $^{\circ}\text{C}$ . For the evaluation of the precious metal dispersion a CO:Pd adsorption ratio of 1:1 is assumed [30]. The measurement of the oxygen storage capacity complete (OSCC) is based on the aftertreatment protocols for catalyst characterization by Rappé et al.

[26]. The monolithic catalyst is oxidized at 550 °C with 2% O<sub>2</sub> in N<sub>2</sub> for 20 min in the test setup described below. Subsequently the sample is cooled down to the temperatures of 550 °C, 350 °C and 150 °C in N<sub>2</sub> and in the following reduced with 1% CO in N<sub>2</sub>. The OSCC at the respective temperature corresponds to the amount of CO<sub>2</sub> formed during reduction and is specified per mass of catalyst.

### 2.3. Testing apparatus and testing routine

The coated honeycomb was tested under steady-state and forced periodic conditions in an in-house built catalyst testing bench that is schematically illustrated in Fig. 1. The monolith was wrapped in quartz glass wool, placed in a quartz glass tubular reactor (19 mm OD, 17 mm ID, 720 mm length, Qsil) and mounted between two thermocouples (1 mm OD, TC Direct) located 5 mm up- and downstream of the monolith that were held in the middle of the reactor by inert cordierite honeycombs. The inlet temperatures of the catalyst could be precisely adjusted via the regulation of the furnace with a Eurotherm controller. The flow of gaseous reactants was supplied by mass flow controllers (MFCs, Bronkhorst). To ensure low-pulsation dosing of water, a controlled evaporation mixing device (CEM, Bronkhorst) was used along with a liquid flow controller (LFC, Bronkhorst).

The static composition of the simulated exhaust gas, which is representative for real-world applications, contained 1330 ppm NO, 360 ppm C<sub>3</sub>H<sub>6</sub>, 180 ppm C<sub>3</sub>H<sub>8</sub>, 10% CO<sub>2</sub> and 13% H<sub>2</sub>O. To avoid condensation of the water vapor in the pipes of the test bench, all pipes were heated to 120 °C with heating wires (Horst). The dosing of the periodic forced components CO, H<sub>2</sub> and O<sub>2</sub> was realized with two fast switching 3-way 2-position valves (Bürkert), which alternately dose the lean and rich mixture into the reactor and the ventilation system, respectively (cf. Table 1). N<sub>2</sub> served as a balancing gas to keep the volume flows constant in both, lean and rich mixtures. A pre-pressure regulator (PR, Equilibar) was used to align the pressure in the exhaust line to that in the reactor. Equation (1) that was first formulated by Padeste and Baiker [24] was used to calculate the AFR from the molar fractions of the individual species, which are shown in Table 1.

$$\lambda = \frac{2[\text{O}_2] + [\text{CO}] + 2[\text{CO}_2] + [\text{H}_2\text{O}] + [\text{NO}]}{2[\text{CO}] + [\text{H}_2] + 2[\text{CO}_2] + [\text{H}_2\text{O}] + 9[\text{C}_3\text{H}_6] + 10[\text{C}_3\text{H}_8]} \quad (1)$$

Steady-state and dithering experiments were conducted at realistic

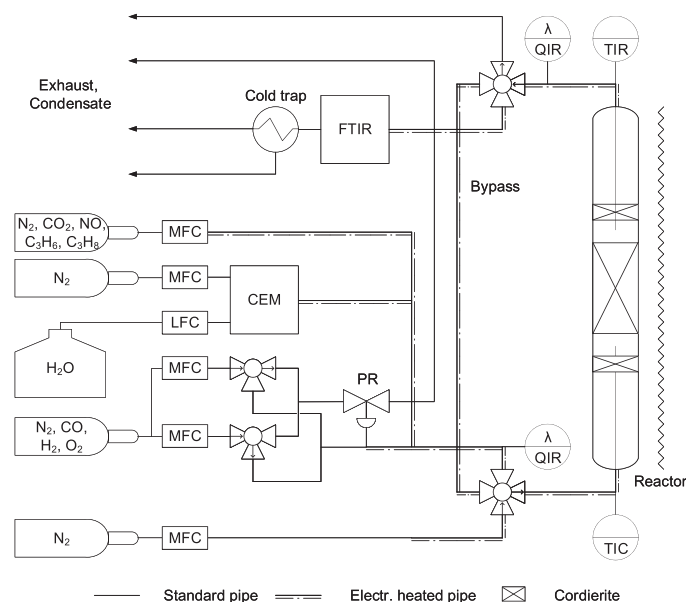


Fig. 1. Scheme of the apparatus used for investigating the influence of operating conditions on the dynamic behavior of the three-way catalyst.

Table 1

Dosed O<sub>2</sub>, CO and H<sub>2</sub> concentrations at different air-fuel equivalence ratios (AFR). Components with constant concentrations: 1330 ppm NO, 360 ppm C<sub>3</sub>H<sub>6</sub>, 180 ppm C<sub>3</sub>H<sub>8</sub>, 10% CO<sub>2</sub> and 13% H<sub>2</sub>O.

Amplitude, mean lambda	$\lambda / -$	[O <sub>2</sub> ] / ppm	[CO] / ppm	[H <sub>2</sub> ] / ppm
A = 0.02, $\lambda_m = 1.00$	1.02	6 500	1 800	600
	0.98	3 000	6 800	2 270
A = 0.04, $\lambda_m = 1.00$	1.04	9 000	800	270
	0.96	1 900	10 500	3 500
A = 0.06, $\lambda_m = 1.00$	1.06	12 200	570	190
	0.94	1 200	15 000	5 000
A = 0.04, $\lambda_m = 0.99$	1.03	7 700	1 100	370
	0.95	1 500	12 700	4 200
A = 0.04, $\lambda_m = 1.01$	1.05	10 500	690	230
	0.97	2 400	8 600	2 900

experimental conditions that are representative for real-world TWC applications [31–33,34,35], namely temperatures  $T = 150$ – $550$  °C, frequencies  $f = 0.0025$ – $2.5$  Hz, gas hourly space velocities  $GHSV = 50$  000– $100$  000 h<sup>-1</sup>, dithering amplitudes  $A = 0.02$ – $0.06$ , split cycles  $s_L = 0.375$ – $0.625$ , which according to Silveston et al. [4] indicates the ratio between the lean cycle period  $\tau_L$  and the cycle period  $\tau$  (cf. Equation (2)), and mean lambda  $\lambda_m = 0.99$ – $1.01$ . The relationship between amplitude, split cycle, mean lambda value and time-average lambda value  $\lambda_\phi$  is shown in Fig. 2.

$$s_L = \frac{\tau_L}{\tau} \quad (2)$$

Furthermore, the influence of the diminishing of the real amplitude  $A_{\text{real}}$  by axial dispersion in the plant periphery was investigated. For this purpose, the velocity of the gas flow in the reactor  $v$  at a constant  $GHSV$  was increased by increasing the monolith length between 3–6 cm and increasing the volume flow by the same factor. The influence of the oxygen storage capacity (OSC) was tested by mixing the 2% Pd/Al<sub>2</sub>O<sub>3</sub> and 2% Pd/CZ in mass ratio of  $x = 40\%$  and  $x = 80\%$  (Pd[(x)CZ/(1-x)Al<sub>2</sub>O<sub>3</sub>]).

The average conversion of the reactants CO, NO<sub>x</sub>, C<sub>3</sub>H<sub>6</sub>, C<sub>3</sub>H<sub>8</sub> (Equation (3)) and the selectivity to the product species NH<sub>3</sub>, N<sub>2</sub>O, NO<sub>2</sub> (Equation (4)), with the respective stoichiometric coefficient  $\nu_i$ , were calculated by time integration of the transient concentration profiles (Equation (5)) measured by an FTIR spectrometer (MultiGas 2030, MKS Instruments) operated at 5 Hz and with a measuring cell volume of 200 mL. The integration time used was chosen to be a multiple  $n$  of the respective cycle time  $\tau$ . AFR sensors (LSU 4.9, Bosch) at the inlet and outlet of the reactor allowed to analyze the dynamics of the lambda changes with a temporal resolution of 10 Hz. The concentration of the IR-inactive species N<sub>2</sub> was calculated from a balance of all nitrogen-containing species, among which NO, NO<sub>2</sub>, N<sub>2</sub>O and NH<sub>3</sub> can be

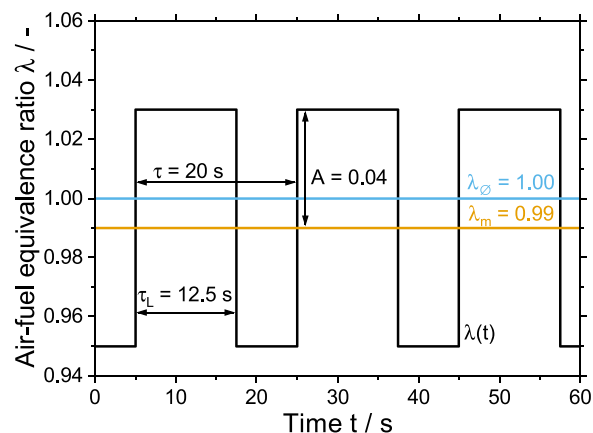


Fig. 2. Relationship between amplitude  $A$ , split cycle (cf. Equation (2)), mean lambda  $\lambda_m$  and time-average lambda  $\lambda_\phi = (1 - s_L) \cdot (\lambda_m - A) + s_L \cdot (\lambda_m + A)$ .

precisely quantified by FTIR.

$$X_i = \frac{\bar{x}_{i,0} - \bar{x}_i}{\bar{x}_{i,0}} \quad (3)$$

$$S_{i,\text{NO}} = \frac{\nu_{\text{NO}}}{\nu_i} \frac{\bar{x}_i - \bar{x}_{i,0}}{\bar{x}_{\text{NO},0} - \bar{x}_{\text{NO}}} \quad (4)$$

$$\bar{x}_i = \frac{1}{n\tau} \int_t^{(t+n\tau)} x(t') dt' \quad (5)$$

### 3. Results and discussions

#### 3.1. Testing apparatus

Prior to the catalytic tests, possible gas phase reactions were investigated by means of a light-off experiment up to 600 °C and a temperature ramp of 3 K min<sup>-1</sup> with an inert honeycomb at stoichiometric condition ( $\lambda_m = 1, A = 0.04$ , cf. Table 1). Figure S1 in the Supplementary Information shows that gas phase reactions of CO, NO, C<sub>3</sub>H<sub>6</sub>, C<sub>3</sub>H<sub>8</sub> can be ruled out in the investigated temperature range.

To validate the experimental system over the wide range of operating conditions, the response of the analytics after a step change in CO concentration was studied using an uncoated monolith at the maximum ( $GHSV = 100\,000\text{ h}^{-1}, T = 550\text{ °C}$ ) and minimum ( $GHSV = 50\,000\text{ h}^{-1}, T = 150\text{ °C}$ ) gas velocities (Fig. 3a). The time lag due to gas transport between the valves and the analytics is 0.1 s for the front and 0.8–1.8 s for the rear AFR sensors, respectively, and 3.2–4.5 s for the FTIR. This time offset could be taken into account on the basis of the volumes, temperatures, and gas velocities in each plant section. The time constant for reaching 90% of the CO concentration after the step change is 0.6–0.9 s for the AFR probes and 2.1–4.6 s for the FTIR. The absolute values of the front AFR sensor for the inert system at a space velocity of 50 000 h<sup>-1</sup> and an amplitude of 0.02 are plotted in Fig. 3b and show that the set amplitude cannot be fully achieved at a frequency of 0.5 Hz and complete mixing of the lean and rich half cycle in front of the reactor occurs at 1 Hz at the present conditions. Notably, the influence of thermocouple attachment with inert mini-monoliths on the back-mixing behavior was ruled out by comparing experiments conducted with and without the inert mini-monoliths (cf. Figure S2).

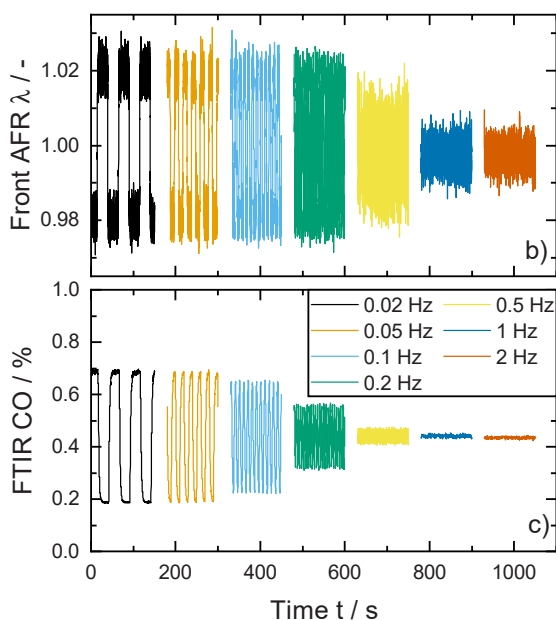
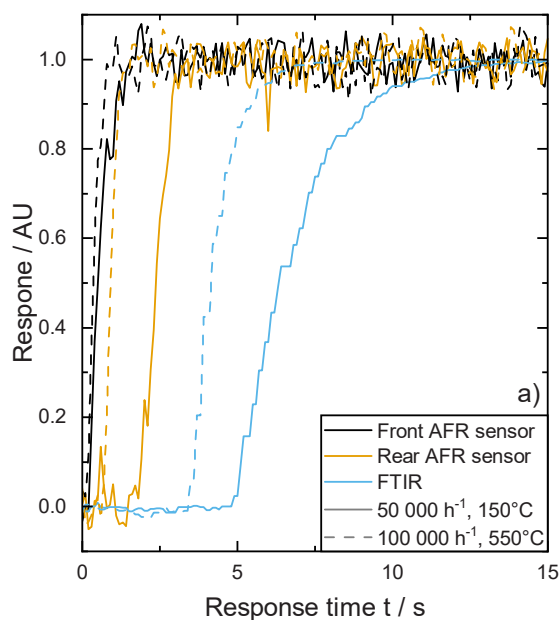


**Fig. 3.** a) Response of AFR sensors and FTIR to a step change of CO concentration using an uncoated monolith at different gas velocities. b) AFR values and c) CO concentrations as a function of time at different frequencies and  $GHSV = 50\,000\text{ h}^{-1}, T = 150\text{ °C}, A = 0.02$ . The exhaust gas composition is listed in Table 1.

Figure 3c shows the concentration profile of CO as a function of time at different frequencies. Due to back-mixing of the gas in the measuring cell volume of the FTIR, the exact concentration profiles exiting the reactor are not available [36]. However, the average concentration of the respective species exiting the reactor over a cycle period can be considered equal to those in the FTIR. In contrast to the results reported by Roger et al. [37], frequency and amplitude had no influence on the average quantity of pulsed components. This could be achieved by avoiding the pressure peak downstream of the MFC when switching between the reactor and the exhaust line [38].

#### 3.2. Influence of temperature

In Fig. 4 the time-averaged conversion of the exhaust gas pollutants and the selectivity to products derived from NO are shown for different frequencies and temperatures at  $GHSV = 75\,000\text{ h}^{-1}$  and  $A = 0.04$ . The quasi steady-state (qss) conversion of the reactants and selectivity of the products for a frequency tending towards zero ( $f \rightarrow 0$ ) was obtained by calculating the arithmetic mean between the outlet concentration of the respective lean and rich steady-state experiments. The theoretical values for quasi steady-state experiments are in agreement with the data from periodic operation for a frequency greater than zero and forms the limit between dynamic and static operation. Another border case is represented for high frequencies, where the square wave inlet signal deteriorates before reaching the catalytic converter due to axial dispersion in the periphery of the test bench. To represent this upper limit ( $f \rightarrow \infty$ ), the composition of the lean and rich mixtures were averaged and fed to the reactor at steady-state conditions. AFR sensor data show that at  $f = 2.5\text{ Hz}, GHSV = 75\,000\text{ h}^{-1}$  and  $A = 0.04$  the square waveform deteriorates almost completely and thus passes into the steady-state case (cf. Fig. 5,  $v = 0.44\text{ m s}^{-1}$ ). The deviations between the data point at an inlet temperature of 300 °C at 2.5 Hz ( $T_{\text{out}} = 383\text{ °C}$ ) and in the steady-state ( $f \rightarrow \infty, T_{\text{out}} = 387\text{ °C}$ ) can be attributed to different temperature profiles along the monolith due to the weak fluctuation and the associated strong influence of the temperature on the conversion during the light-off. However, the set amplitude and  $GHSV$  can significantly influence the back-mixing behavior between the two half cycles, which will be discussed in more detail in the next sections.

For temperatures below 350 °C, there is an optimum frequency at which C<sub>3</sub>H<sub>8</sub> and NO conversion reach a maximum. Compared to

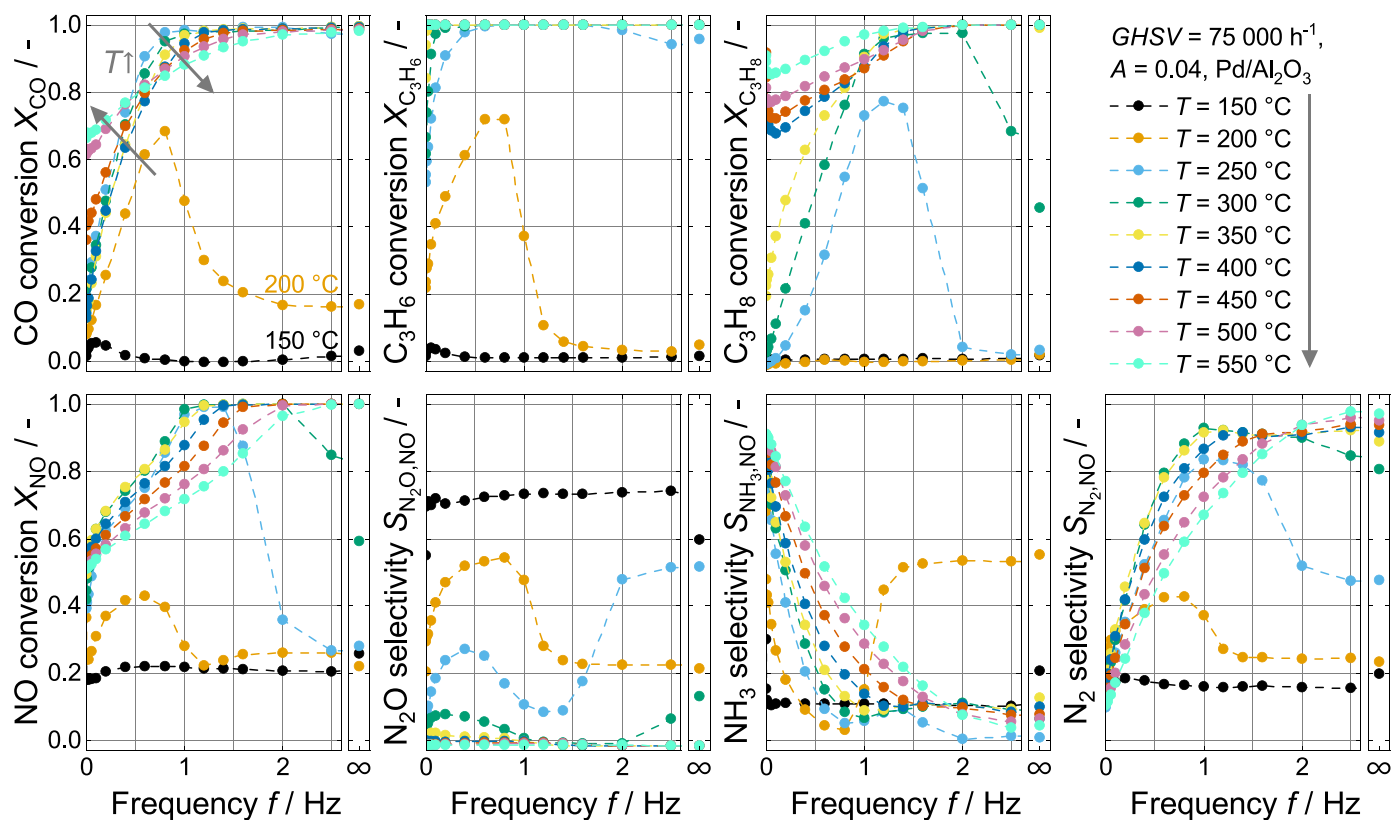


Fig. 4. Average conversion of pollutants and selectivity of products formed from NO at different frequencies and temperatures at constant  $GHSV = 75\,000\text{ h}^{-1}$ ,  $A = 0.04$  on  $\text{Pd}/\text{Al}_2\text{O}_3$ . The exhaust gas composition is listed in Table 1.

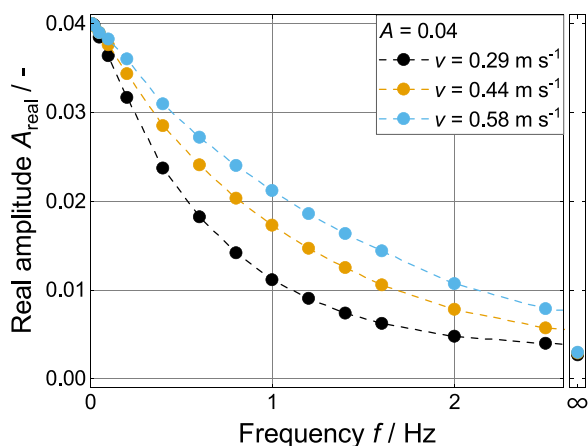


Fig. 5. Real amplitudes in front of the catalyst at different frequencies and gas velocities in the tubular reactor at constant  $A = 0.04$  measured by the front AFR sensor. The gas velocities of  $v = 0.29$ ,  $0.44$  and  $0.58\text{ m s}^{-1}$  correspond to  $GHSV = 50\,000$ ,  $75\,000$ ,  $100\,000\text{ h}^{-1}$  for a monolith length of  $3\text{ cm}$ .

negligible conversions at steady-state, 80% of  $\text{C}_3\text{H}_8$  can already be converted at a temperature of  $250\text{ }^\circ\text{C}$  and a frequency of  $1.2\text{ Hz}$  in the periodic operation.  $\text{CO}$  and  $\text{C}_3\text{H}_6$ , on the other hand, exhibit optimal frequencies already in a lower temperature range (below  $300\text{ }^\circ\text{C}$ ) since their light-offs generally occur at lower temperatures [39]. The C-H bond activation of different hydrocarbons on (noble) metal catalysts strongly depends on the type of hydrocarbon (i.e. saturated vs. unsaturated, short-chain or long-chain), temperature and reaction mixture [40]. In general, alkenes adsorb strongly, whereas the adsorption of alkanes is weaker in competition with oxygen on metal-based catalysts, which results in a higher reactivity of the unsaturated hydrocarbon [40,

41].

In case of a stoichiometric steady-state operation, the reaction rate at low temperatures is inhibited by the uneven distribution of reactants on the catalyst surface. It is well known that during  $\text{CO}$  oxidation  $\text{Pt}$  and  $\text{Pd}$  catalysts suffer from self-poisoning by either  $\text{CO}$  or  $\text{O}_2$  [42,43], depending on the stoichiometry of the particular reaction mixture [14, 44]. Moreover, it was demonstrated that hydrocarbons can similarly inhibit the reaction rate of the catalyst through self-poisoning [14,15].

As the temperature increases, the optimal frequency to achieve the highest conversion for all pollutants increases. Therefore, the optimal frequency for  $\text{NO}$  and  $\text{C}_3\text{H}_8$  conversion increases from  $0.8\text{ Hz}$  at  $200\text{ }^\circ\text{C}$  to  $1.2\text{ Hz}$  at  $250\text{ }^\circ\text{C}$  and to  $1.6\text{ Hz}$  at  $300\text{ }^\circ\text{C}$ . Similarly, Muraki et al. [5] observed an increase in the optimum frequency for pollutant conversion with increasing temperature over a  $0.05\text{ g L}^{-1}$   $\text{Pd}/\text{Al}_2\text{O}_3$  catalyst operated under net stoichiometric conditions. However, they noted optimal frequencies at much higher temperatures, which is probably due to the low  $\text{Pd}$  loading of their samples as well as differences in the reaction conditions and the plant periphery.

To understand the periodic effect on a molecular level it is useful to examine lean-rich and rich-lean step changes of a simpler system. Barshad and Gulari [45] observed a temperature-dependent induction time after  $\text{O}_2$  was introduced to preadsorbed  $\text{CO}$  on  $\text{Pd}/\text{Al}_2\text{O}_3$ .  $\text{CO}$  has to desorb and vacate some active sites before  $\text{O}_2$  can adsorb and react. This time lag was found to correspond to the minimum time period that is needed for rate enhancement under periodic operation [46]. Since  $\text{CO}$  desorption is a temperature-activated process, the induction time can be reduced with increasing temperature, which leads to a quicker time of reaching the optimum surface coverage on the catalyst after the rich to lean switch. Hence, higher frequencies are necessary to maintain an equal quantity of the reactants on the surface of the catalyst.

In addition to the increase in the reaction rate in periodic operation due to equalizing of the reactant composition on the catalyst, the temperature in the monolithic catalyst also increases as a result of the

increasing amount of heat of reaction that is released. The time-averaged temperature difference between the monolith inlet and outlet at  $T = 200\text{ }^{\circ}\text{C}$ ,  $GHSV = 75\ 000\ \text{h}^{-1}$  and  $A = 0.04$  is shown in Fig. 6 at different frequencies. The optimal frequency of 0.8 Hz for the maximum conversion of the pollutant (cf. Fig. 4, orange graph) matches the frequency of the maximum average temperature difference. Self-amplification of the system occurs as the reaction rate continues to increase due to the higher average temperature in the monolith. Jaree et al. [47] observed temperature jumps above the adiabatic combustion temperature when changing the inlet CO concentration on Pt/Al<sub>2</sub>O<sub>3</sub> and attributed it to segregation of mass and heat waves moving through the reactor during periodic operation, which are induced by CO self-inhibition.

At temperatures above 350 °C, complete conversion of all exhaust gas components takes place during stoichiometric steady-state operation, whereas periodic operation at low frequency results in a worse catalyst performance (cf. Fig. 4). Silveston [4] showed that the optimal cycle period and rate enhancement of periodic operation for CO oxidation on noble metals decrease with increasing temperature. As a result of CO desorption at higher temperatures, the distribution of reactants on the catalyst surface already becomes evenly distributed during steady-state operation. Consequently, lean-rich cycling cannot enhance the reaction rate any further [48].

Furthermore N<sub>2</sub>O formation was observed during steady-state stoichiometric operation in a temperature range of 150–300 °C (black, orange, light blue, green lines in Fig. 4). Mejía-Centeno et al. [49] investigated a Pd-only TWC and reported the formation of N<sub>2</sub>O between 100–320 °C as well as the formation of NH<sub>3</sub> in a temperature range of 320–550 °C, which is correlated to the H<sub>2</sub> production via the stream reforming process. The formation of N<sub>2</sub>O is discussed in more detail in the following sections of the present study.

Deviating from the study mentioned above, in our experiments additional NH<sub>3</sub> formation was observed in a lower temperature range from 150 °C to 200 °C, which was attributed to the low-temperature activation of H<sub>2</sub> [50] and can also be observed for slightly lean feed composition [51]. NO<sub>2</sub> selectivities fall below the 5% mark and are therefore not illustrated in Fig. 4. However, the absolute emission of all nitrogen species for temperatures between 200 °C and 300 °C are shown in Fig. 7. Steady-state lean and rich experiments allow to attribute the formation of high quantities of NO<sub>2</sub> and NH<sub>3</sub> at low frequencies to long periods in the lean and rich phase, respectively. Under lean conditions ( $\lambda = 1.04$ ), the excess oxygen on the catalytic surface oxidizes NO to NO<sub>2</sub>. In contrast, the higher amounts of hydrogen that are present in the feed gas mixture under rich conditions ( $\lambda = 0.96$ ), result in an increased formation of NH<sub>3</sub>.

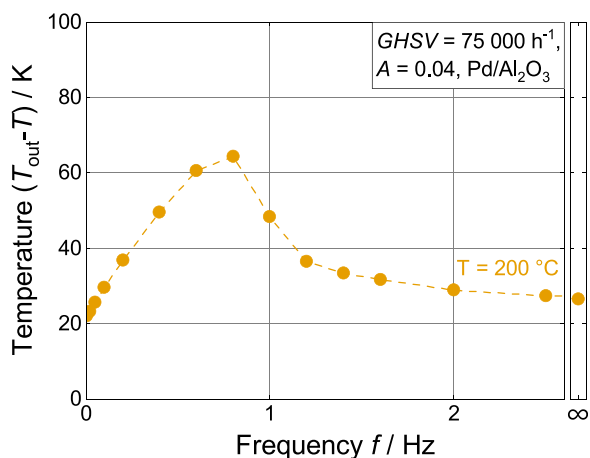


Fig. 6. Average temperature difference between inlet and outlet of the monolith at  $T = 200\text{ }^{\circ}\text{C}$ ,  $GHSV = 75\ 000\ \text{h}^{-1}$ ,  $A = 0.04$  on Pd/Al<sub>2</sub>O<sub>3</sub>. The exhaust gas composition is listed in Table 1.

As underscored by the selectivities of the NO reduction products, the optimum frequency, and thus the optimum composition on the catalyst surface for the conversion of the pollutants, does not always correspond to low secondary emissions of NH<sub>3</sub> and N<sub>2</sub>O. For instance, the N<sub>2</sub>O selectivity reaches a maximum at a temperature of 200 °C and a frequency of 0.8 Hz, which is the optimal operating point for the maximum conversion of CO, C<sub>3</sub>H<sub>6</sub> and NO. Simultaneously, the low-temperature NH<sub>3</sub> formation observed when operating the catalyst under constant feed conditions can be prevented.

In contrast, at temperatures of 250 °C and 300 °C, the selectivity toward N<sub>2</sub>O can be reduced at the respective optimal frequencies of 1.2 Hz and 1.6 Hz, while NH<sub>3</sub> production increases. In conclusion, the formation of the secondary products NH<sub>3</sub> and N<sub>2</sub>O shifts to lower temperatures upon periodic catalyst operation. This is in line with results by Padeste and Baiker [24] who reported a shift of N<sub>2</sub>O formation to lower temperatures in periodic mode during light-off experiments. Nevertheless, by providing optimal fluctuations in a temperature range between 200 °C and 350 °C the selectivity to NH<sub>3</sub> and N<sub>2</sub>O can be significantly reduced and therefore the N<sub>2</sub> selectivity can be increased by up to 30% compared to steady-state operation.

### 3.3. Influence of oxygen storage capacity

Figure 8 shows the influence of the temperature on the time-averaged pollutant conversion and the product selectivity at  $A = 0.04$ , and  $GHSV = 75\ 000\ \text{h}^{-1}$  on the Pd/CZ catalyst. At steady-state conditions, Pd/CZ shows a similar conversion temperature behavior as the Pd/Al<sub>2</sub>O<sub>3</sub> catalyst (cf. Fig. 4) regarding CO, C<sub>3</sub>H<sub>6</sub> and C<sub>3</sub>H<sub>8</sub> conversion, whereas the NO conversion is decreased at temperatures up to 200 °C. For higher temperatures, NO conversion is shown to be similar to that of the Pd/Al<sub>2</sub>O<sub>3</sub> catalyst.

The comparable activity of the Al<sub>2</sub>O<sub>3</sub>- and CZ-supported catalysts regarding the conversion of CO, NO and HC observed herein is in contrast to the lower light-off temperatures for CO and higher light-off temperatures for HC and NO reported in previous studies [49,52] when CZ is used as support material for Pd. Thus, in order to understand their behavior in more detail, the catalysts investigated in the present study were characterized. Table 2 summarizes the BET surface area and pore volume as determined by means of N<sub>2</sub>-physisorption, the Pd mass fraction that was determined by means of elemental analysis, the reduction temperatures obtained by means of H<sub>2</sub>-TPR measurements, and the average Pd nanoparticle size that was obtained based on STEM measurements. Despite its lower surface area and pore volume, the Pd/CZ sample exhibits slightly smaller Pd particles of 3.7 nm (compared to 4.4 nm for Pd/Al<sub>2</sub>O<sub>3</sub>). Possibly, the ceria-containing support facilitates the dispersion of palladium due to strong noble metal support interactions that have been reported for ceria-supported Pt, Pd, and Ru catalysts [53–55]. Furthermore, the lower Pd reduction temperature that was measured by H<sub>2</sub>-TPR suggests a higher reducibility of Pd in Pd/CZ sample compared to Pd/Al<sub>2</sub>O<sub>3</sub>, which is also attributed to the strong interaction between the noble metal Pd and the CZ support. Notably, a second peak during H<sub>2</sub>-TPR has been observed at 40 °C, which can be attributed to the reduction of CeO<sub>2</sub> of the Pd/CZ sample [56]. Analogous to the well-known noble metal particle size dependencies of CO and NO oxidation over lean-operated oxidation catalysts [57,58], the activity of TWCs is strongly governed by their noble metal particle size and the reducibility of the support [59,60] and thus explains the differences in catalytic activity between Pd/Al<sub>2</sub>O<sub>3</sub> and Pd/CZ. In conclusion, these beneficial properties of the Pd/CZ catalyst enable a similar catalytic activity compared to Pd/Al<sub>2</sub>O<sub>3</sub>, although the latter one has a slightly higher noble metal loading. This becomes particularly clear when comparing the turnover frequencies (TOF) of the pollutant conversion for both catalysts at stoichiometric steady-state conditions (Figure S3), which is based on the respective active catalytic surface area that was derived from the characterization data (Table 2): In terms of TOF, Pd/CZ is slightly more active for CO, HC and NO emissions

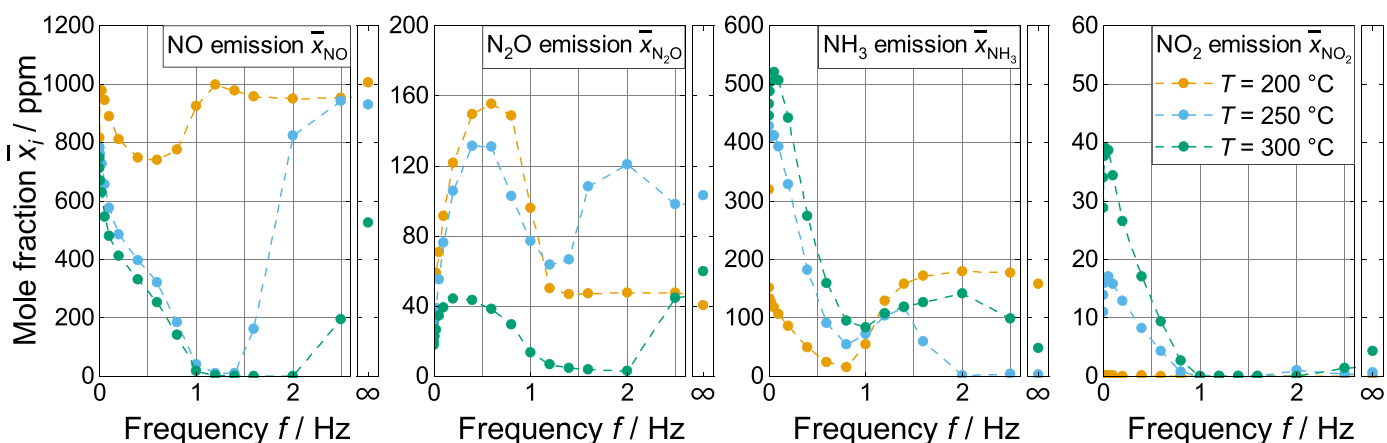


Fig. 7. Average emissions of nitrogenous species at different frequencies and temperatures at constant  $GHSV = 75\,000\text{ h}^{-1}$ ,  $A = 0.04$  on Pd/Al<sub>2</sub>O<sub>3</sub>. The exhaust gas composition is listed in Table 1.

abatement than Pd/Al<sub>2</sub>O<sub>3</sub> under most conditions. Only regarding NO conversion at low temperatures, Pd/Al<sub>2</sub>O<sub>3</sub> outperforms Pd/CZ. The reduced NO conversions (c.f. Fig. 8) and turnover frequencies (c.f. Figure S3) at low temperatures suggest that the selective catalytic reduction of NO with H<sub>2</sub> on Pd/CZ is reduced compared to Pd/Al<sub>2</sub>O<sub>3</sub> and H<sub>2</sub> is already oxidized with O<sub>2</sub> at lower temperatures. Thus, lower selectivities to NH<sub>3</sub> can be observed at 200 °C for the CZ-based Pd catalyst. In agreement with the data of alumina-based sample, Pd/CZ shows N<sub>2</sub>O formation in a temperature range of 150–300 °C and NH<sub>3</sub> formation in a temperature range of 300–550 °C.

In contrast to the steady-state conditions, the pollutant conversions and product selectivities of the CZ- and aluminum-based Pd samples differ in periodic operation. In particular, Pd/CZ can achieve higher conversion of the pollutants compared to Pd/Al<sub>2</sub>O<sub>3</sub> at high temperature and low frequencies. This can be attributed to the OSC of CeO<sub>2</sub> in the Pd/CZ sample, which can reduce the CO, C<sub>3</sub>H<sub>6</sub> and C<sub>3</sub>H<sub>8</sub> slip under pronounced rich conditions and the NO slip under pronounced lean conditions. O<sub>2</sub> exchange between Pd and ceria can take place due to spill-over reactions at the interface of Pd as noble metal and the support [61]. Furthermore, under rich conditions, ceria was reported to be in a reduced state and covered by carbonate species, which can be removed after re-oxidation [62]. This indicates that ceria is capable of providing both oxidizing and reducing agents for rich and lean phases, respectively.

Figure 9 shows the influence of different CZ mass fractions on the time-averaged conversion of the exhaust gas pollutants and the selectivity to products derived from NO at  $A = 0.04$ ,  $GHSV = 75\,000\text{ h}^{-1}$  and  $T = 250\text{ °C}$ . With increasing CZ mass fraction, the N<sub>2</sub>O selectivity decreases and the N<sub>2</sub> selectivity increases at steady-state conditions. This can be attributed to the higher reducibility of Pd/CZ, which was uncovered by our H<sub>2</sub>-TPR measurements (cf. Table 2) and which has previously been associated with a higher N<sub>2</sub>O decomposition activity of the supported noble metal [63]. In dynamic operation, an increase in the CZ mass fraction in the washcoat leads to a shift in the pattern of pollutant conversions and product selectivities to lower frequencies. This is consistent with observations on Pt-Rh based catalysts with variable CeO<sub>2</sub> content [64]. Padeste and Baiker [24] attribute the three times lower optimum frequency of Pt-Rh/CeO<sub>2</sub>-Al<sub>2</sub>O<sub>3</sub> compared to Pt-Rh/Al<sub>2</sub>O<sub>3</sub> to a higher effective storage capacity if the respective catalyst is operated under the optimum frequency.

Figure 10 shows AFR sensor data before and after catalysts with different CZ mass fraction after a rich-lean switch (left) and a lean-rich switch (right) at  $A = 0.04$ ,  $GHSV = 75\,000\text{ h}^{-1}$  and  $T = 300\text{ °C}$ . The OSC under dynamic conditions cannot be quantitatively determined in our experiments using the data of the AFR probes. However, the ratio between the integral values of Fig. 10 and the maximal theoretical values

of complete transition from Pd<sup>+I</sup>/Ce<sup>+IV</sup> to Pd<sup>0</sup>/Ce<sup>+III</sup> (cf. Table 3) are in good agreement. Nevertheless, it can be assumed that the dynamic oxygen storage capacity in our experiments is lower than the OSCC measured by reduction with CO. This can be attributed to the presence of H<sub>2</sub>O and CO<sub>2</sub>, which lowers the reductive chemical potential [65]. On the other hand, a lower oxygen storage capacity can be observed under transient conditions due to transfer limitations of oxygen [66]. With increasing mass fraction of CZ, the time to reach the steady-state after a switch of conditions increases, due to the higher OSC (Fig. 10). As a result, the time at which the optimum reactant composition is present on the catalyst after a step change increases, thus lowering the optimum frequency. This is consistent with the dynamic oxygen storage capacity experiments of Shen et al. [52], which showed a shift of the CO<sub>2</sub> concentration peak to higher times when using Pd/CZ instead of Pd/Al<sub>2</sub>O<sub>3</sub>.

### 3.4. Influence of split cycle

Figure 11 shows the influence of the split cycle on time-averaged pollutant conversion and product selectivity at  $T = 250\text{ °C}$ ,  $A = 0.04$ , and  $GHSV = 75\,000\text{ h}^{-1}$ . Since the optimum frequencies for all species are strongly pronounced at 250 °C, this temperature was chosen for further investigation of the operating conditions. To obtain time-averaged lambda values between 0.99 and 1.01, the split cycle was varied accordingly between  $s_L = 0.375$ –0.625. In steady-state and quasi steady-state, a higher oxygen content due to higher time-averaged lambda values leads to an increased conversion of CO and C<sub>3</sub>H<sub>6</sub>. In contrast, C<sub>3</sub>H<sub>8</sub> and NO conversions do not profit from the higher AFR. This can be attributed to the low temperature of 250 °C in this experiment at which no steam reforming processes occur. Notably, the product distribution of secondary emissions shifts to high N<sub>2</sub>O selectivity and low NH<sub>3</sub> selectivity for increasingly lean conditions. NH<sub>3</sub> formation can be enhanced by high H<sub>2</sub> concentrations, while N<sub>2</sub>O formation occurs at low temperatures under oxygen-rich conditions [39]. In this context, N<sub>2</sub>O emissions were attributed to the formation of NCO surface intermediates formed by the reaction of adsorbed CO and NO [67].

Interestingly, the optimal frequency for CO and C<sub>3</sub>H<sub>6</sub> conversion and NH<sub>3</sub> selectivity shifts to higher frequencies with increasing split cycle. This is consistent with the data of Barshad and Gulari [68] who observed a longer optimal cycle period when decreasing the split cycle during the periodic operation of CO oxidation on alumina-supported palladium. From the linear relationship between split cycle and the respective optimal frequency (Equation (2)), an optimal time in the lean half cycle of 0.42 s can be determined from Fig. 11 for a maximal CO conversion. Similar to our results, Muraki et al. [12] found a linear relationship between the optimal cycle period and the stoichiometric number, which was manipulated by split cycle variation for NO reduction with CO on a

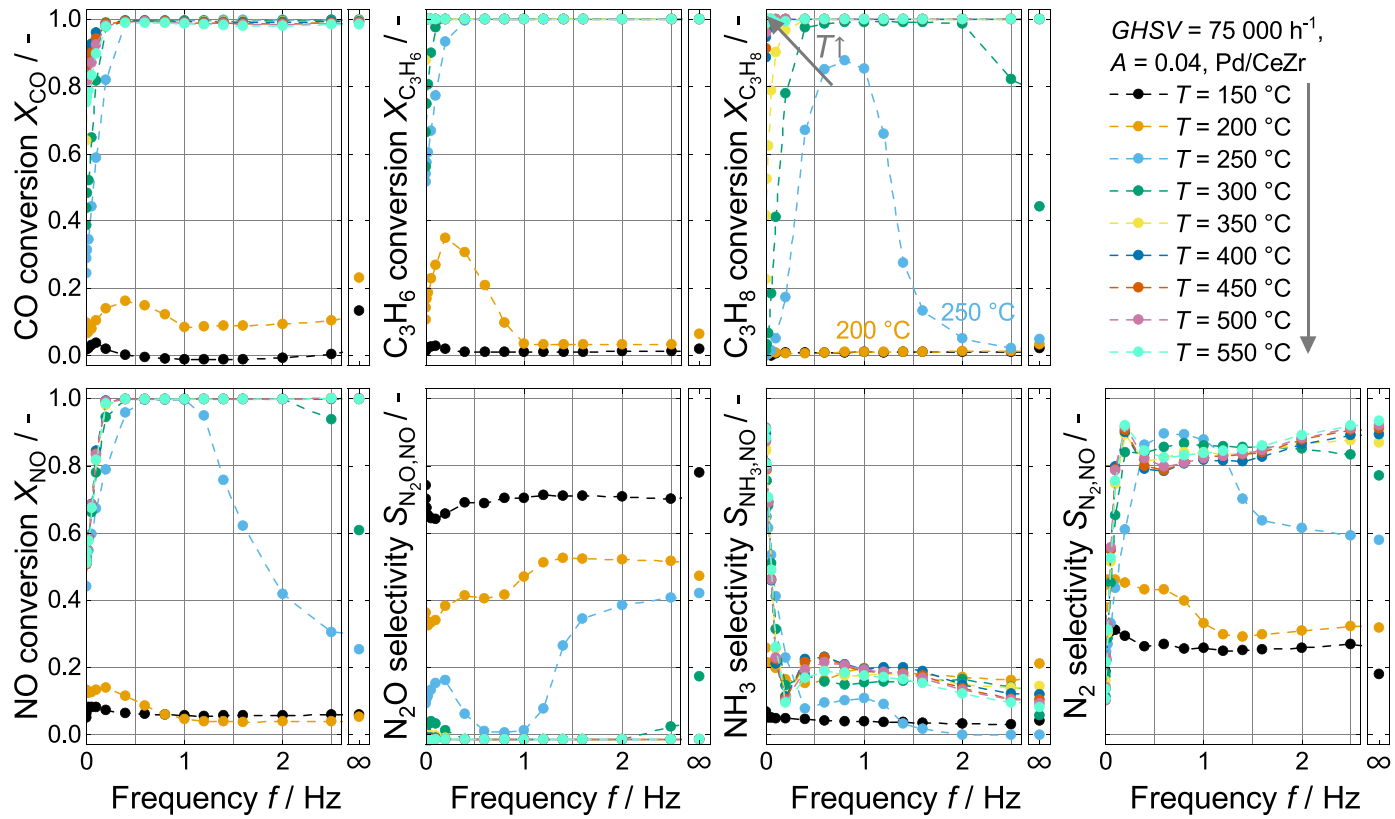


Fig. 8. Average conversion of pollutants and selectivity of products formed from NO at different frequencies and catalyst lengths at constant  $GHSV = 75\,000\text{ h}^{-1}$ ,  $A = 0.04$  on Pd/CZ. The exhaust gas composition is listed in Table 1.

**Table 2**  
Characterization results of Pd/Al<sub>2</sub>O<sub>3</sub> and Pd/CZ.

Properties	Pd/Al <sub>2</sub> O <sub>3</sub>	Pd/CZ
BET surface area $S_{\text{BET}} / \text{m}^2 \text{g}^{-1}$	147	72
Pore volume $v_{\text{pore}} / \text{cm}^3 \text{g}^{-1}$	0.95	0.41
Pd content $x_{\text{Pd}} / \text{wt.-%}$	2.0	1.5
H <sub>2</sub> reduction temperature $T_{\text{Red.H}_2\text{-TPR}} / ^\circ\text{C}$	9	2, 40
Pd nanoparticle diameter $d_{\text{Pd}} / \text{nm}$	$4.4 \pm 1.8$	$3.7 \pm 0.8$

#### Pd/Al<sub>2</sub>O<sub>3</sub> catalyst.

The optimal lean period corresponds to the induction time for desorption of CO from the catalyst surface [45,69]. At this point, the surface concentration of the reactants is balanced and free surface sites are available for further adsorption. If the optimal lean time is exceeded (at low frequencies), the effectiveness of the periodic operation is reduced by excessively long stationary holding times at conditions that inhibit the reaction, namely CO poisoning at rich and O poisoning at lean conditions. If the optimal lean period is not reached (at high frequencies), the catalyst cannot be regenerated from CO poisoning in theory. In reality, however, the frequency is so high that the two gas compositions mix before reaching the catalyst [70]. Maintaining the optimum time at the lean half cycle and increasing the time of the rich half cycle (decrease in split cycle) will therefore result in a decreased maximum CO and C<sub>3</sub>H<sub>6</sub> conversion and an increased NH<sub>3</sub> selectivity, as underscored by our experimental results (cf. Fig. 11). Based on the optimal lean half cycle time found herein, we assume that the time scale of the surface processes for lean-rich switches is considerably smaller than for rich-lean switches for the reaction of CO and C<sub>3</sub>H<sub>6</sub>, and therefore has no effect on the periodic operation. Notably, the dissociative adsorption of oxygen on a CO-poisoned noble metal is inhibited, whereas a noble metal surface covered with oxygen can adsorb considerable amounts of CO [71,72]. For instance, Hegedus et al. [7]

report response times for CO adsorbate formation and removal of 2 s and 1.1 s after a change from lean to rich and from rich to lean, respectively.

In contrast to the behavior of CO, C<sub>3</sub>H<sub>6</sub> and NH<sub>3</sub> in our experiments, the patterns for NO and C<sub>3</sub>H<sub>8</sub> conversion and N<sub>2</sub>O as well as N<sub>2</sub> selectivity shift to lower frequencies when the split cycle is increased or decreased from the symmetric case  $s_L = 0.5$ . Thus, we conclude that by varying the split cycle, both an optimal time in lean and an optimal time in rich conditions exist and can affect the frequency for the maximum conversion of NO and C<sub>3</sub>H<sub>8</sub> as well as the product formation of N<sub>2</sub>O and N<sub>2</sub>. We determine optimal times of 0.48 s and 0.51 s of the lean and rich half cycle, respectively, which is consistent with the maximum NO conversion under slightly rich conditions ( $s_L = 0.4375$ ). However, we can only speculate about the reasons for the optimal times for lean and rich half cycle. NO adsorption and dissociation are possibly enhanced by the release of surface sites during CO desorption after the rich-lean switch. This also applies to the other reactants, which is indicated by the same optimum frequencies of the various pollutant gases. On the other hand, after the lean-rich switch many other mechanisms come into play. For instance, NO dissociation was suggested to be the rate-determine step at high CO coverage of the noble metal [73]. An inhibition of NO dissociation decelerates the formation of NCO [7,74], which is an important surface intermediate in the formation of N<sub>2</sub>O [67]. Since under lean conditions the O<sub>2</sub> concentration is about 5 to 10 times higher than the NO concentration, a more plausible explanation is the competitive adsorption between the weakly bound propane and O<sub>2</sub> [15] due to O poisoning of the catalytic surface, which might yield free surface sites for NO adsorption on the lean half cycle. Hence, O<sub>2</sub> would first have to desorb in a lean-rich switch before propane can adsorb on the surface, similar to the preceding desorption of CO after a rich-lean switch.

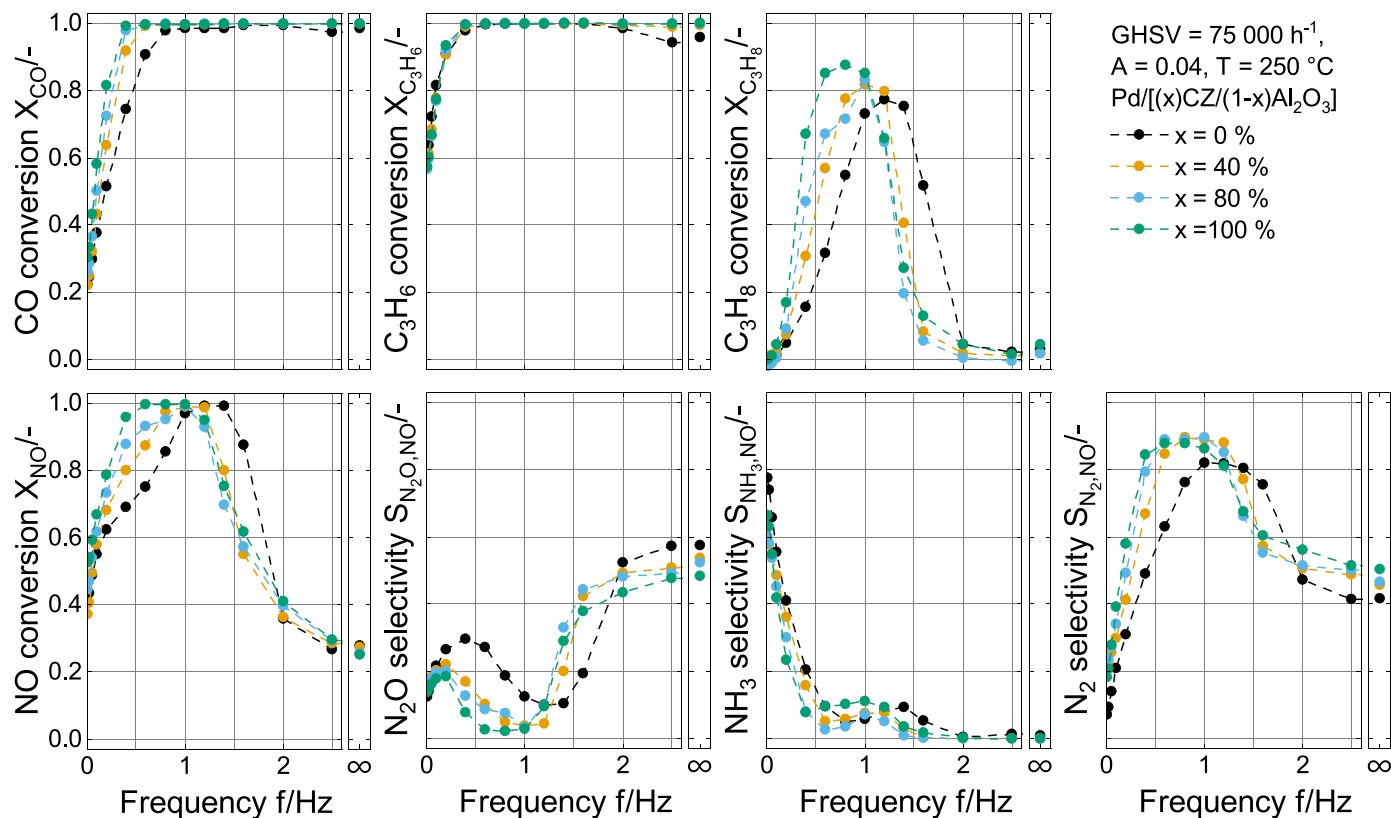


**Fig. 9.** Average conversion of pollutants and selectivity of products formed from NO at different frequencies and CZ mass fractions at constant  $GHSV = 75\,000 \text{ h}^{-1}$ ,  $T = 250 \text{ }^\circ\text{C}$ ,  $A = 0.04$ . The exhaust gas composition is listed in Table 1.

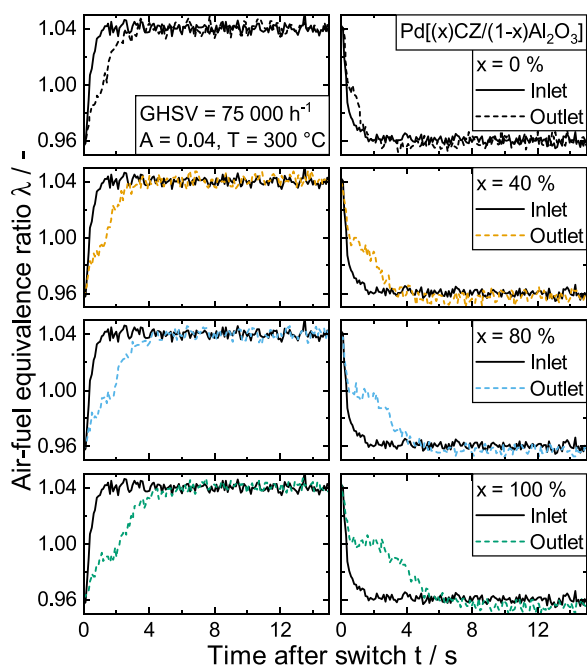


**Fig. 10.** Air-fuel equivalence ratio (AFR) at the inlet and outlet of the reactor after a rich-lean switch (left) and lean-rich switch (right) for different CZ mass fractions recorded by the front and rear AFR sensors at constant  $GHSV = 75\,000\text{ h}^{-1}$ ,  $T = 300\text{ °C}$ ,  $A = 0.04$ . The exhaust gas composition is listed in Table 1.

**Table 3**

Oxygen storage capacity complete (OSCC) for different mass fractions of CZ at different temperatures and the maximal theoretical values of complete transition from  $\text{Pd}^{+1}/\text{Ce}^{+IV}$  to  $\text{Pd}^0/\text{Ce}^{+III}$ .

Pd/[ (x)CZ/(1-x)Al <sub>2</sub> O <sub>3</sub> ]	OSCC / $\mu\text{mol g}^{-1}$ at:			
	150°C	350°C	550°C	max.
x = 0%	76	56	183	189
x = 40%	219	440	440	559
x = 80%	282	687	729	951
x = 100%	310	771	922	1215

### 3.5. Influence of amplitude and mean lambda

The influence of different amplitudes and mean lambda values on the conversion of the exhaust gas and the selectivity to secondary products at  $GHSV = 75\,000\text{ h}^{-1}$  and  $T = 250\text{ °C}$  are shown in Figures 12 and 13, respectively. The amplitude and mean lambda influence the inlet partial pressure of  $\text{O}_2$ ,  $\text{H}_2$  and  $\text{CO}$  at the respective half cycle, as shown in Table 1. The steady-state and quasi steady-state conversions for different amplitudes and mean lambda can be described using a scheme developed by Kang et al. [75] for  $\text{O}_2$  modulation during  $\text{CH}_4$  oxidation over a Pt-Pd/ $\text{Al}_2\text{O}_3$  catalyst. The reaction rate for a species passes through a maximum when plotted against the partial pressure of a modulated species. By slowly modulating the lambda value, a quasi steady-state ( $f \rightarrow 0$ ) is reached and the reaction rate can be higher or lower compared to the steady-state ( $f \rightarrow \infty$ ) depending on the position of the maximum reaction rate and the respective amplitude and mean lambda. However, the reaction rates under full transient conditions can even exceed the reaction rates of the steady-state and quasi steady-state.

The results of the AFR sensor show that at frequencies above 0.4 Hz the set amplitudes are no longer fully achieved (cf. Fig. 3). However, for large amplitudes much higher frequencies are needed to completely mix both half cycles. The difference between the conversions of steady-state ( $f \rightarrow \infty$ ) in Fig. 12 and the highest measured frequency for an amplitude of 0.06 (blue data points in Fig. 12) illustrates this effect. Thus, the

optimal frequency and maximal pollutant conversion also depends on the plant geometry or exhaust tract. Therefore, it is of tremendous importance to specify not only the respective operating conditions in the reactor, but also the residence time distribution when comparing results from different measuring setups.

When the amplitude is increased, the pattern of the pollutant conversion and product selectivities are shifted to higher frequencies. This is in line with individual measurements on Pd- or Pt-based catalysts from the literature [5,24,76]. For the discussion of the influences of the reactant partial pressures on the optimal frequency, it is again useful to consider lean-rich and rich-lean step switches. Increasing the amplitude leads to an increase in the  $\text{O}_2$  and  $\text{CO}$  partial pressure difference between rich and lean phase. Therefore, the transition between an O- and CO-inhibited surface and vice versa is faster. Since the induction time is shorter, higher frequencies are required to regenerate the catalyst from its surface-poisoned state. In our measurement campaign, an increase of the amplitude from 0.02 to 0.04 resulted in the largest increase of the optimal frequency from 0.6 Hz to 1.2 Hz. A further increase of the amplitude to 0.06 leads to an optimum frequency of 1.4 Hz. Possibly, the influence of a further increase of the partial pressure difference of  $\text{CO}$  and  $\text{O}_2$  on the surface inhibition diminishes due to a complete saturation of the surface at the respective inhibiting condition. The conversion of the pollutants at the optimum frequency increases with the increase of the average partial pressure of the reactants, since the reaction under these conditions is no longer inhibited by the uneven distribution of surface adsorbates.

For the variation of the mean lambda value, a similar behavior on the optimal frequency of all species as for the split cycle was found. At first glance, only the time-average lambda plays a role in determining the optimal frequency. However, similar to a change in amplitude, a change in the mean lambda value influences the partial pressure of the reactants and therefore their surface coverage on the catalyst. A decrease of the mean lambda values leads to an increase in the  $\text{CO}$  partial pressures and therefore the surface coverage of  $\text{CO}$  at rich conditions, while the  $\text{CO}$  partial pressure difference between the rich and lean phases increases only slightly. It was shown by Banse et al. [69] that increasing the amount of pre-adsorbed  $\text{CO}$  on a poly-crystalline platinum foil increased the induction time for  $\text{CO}_2$  formation after a rich-lean switch. This is in agreement with the observed decrease in the optimal frequency of  $\text{CO}$  conversion when decreasing the mean lambda value (cf. Fig. 13).

On the other hand, the  $\text{C}_3\text{H}_8$  decomposition depends both on the lean-rich and rich-lean switch as demonstrated by Carlsson et al. [15] by means of  $\text{O}_2$  pulsing experiments on Pt/ $\text{Al}_2\text{O}_3$ , during which two minima of  $\text{C}_3\text{H}_8$  concentration were found within one period [15]. The different behavior for the optimal frequency of  $\text{C}_3\text{H}_8$  and  $\text{NO}$  conversion, namely decreasing optimal frequency with increase and decrease in the mean lambda value from  $\lambda_m = 1$ , is determined by the slower of the two desorption steps after the input conditions are changed. A decrease of the mean lambda value results in a slower  $\text{CO}$  desorption step, whereas an increase of the mean lambda slows down the  $\text{O}$  desorption step. In both cases, the optimal frequency of  $\text{C}_3\text{H}_8$  and  $\text{NO}$  is shifted to lower values.

### 3.6. Influence of GHSV

Although the velocity of the exhaust gas and thus the  $GHSV$  is subject to large fluctuations during real-world driving cycles, to the best of our knowledge no studies on the influence on periodic operation of TWC have been reported. Therefore, Fig. 14 shows the time-averaged conversion of exhaust gas pollutants and the selectivity of the products over the Pd/ $\text{Al}_2\text{O}_3$  catalyst for different frequencies and  $GHSV$ s at  $A = 0.04$  and  $T = 250\text{ °C}$ . In the steady-state and quasi steady-state cases, no clear trend regarding the impact of space velocity on pollutant conversion and product distribution can be observed. This can be attributed to a temperature increase due to an increasing amount of released heat of reaction at higher  $GHSV$ : At a  $GHSV$  of  $75\,000\text{ h}^{-1}$  an increase in the outlet

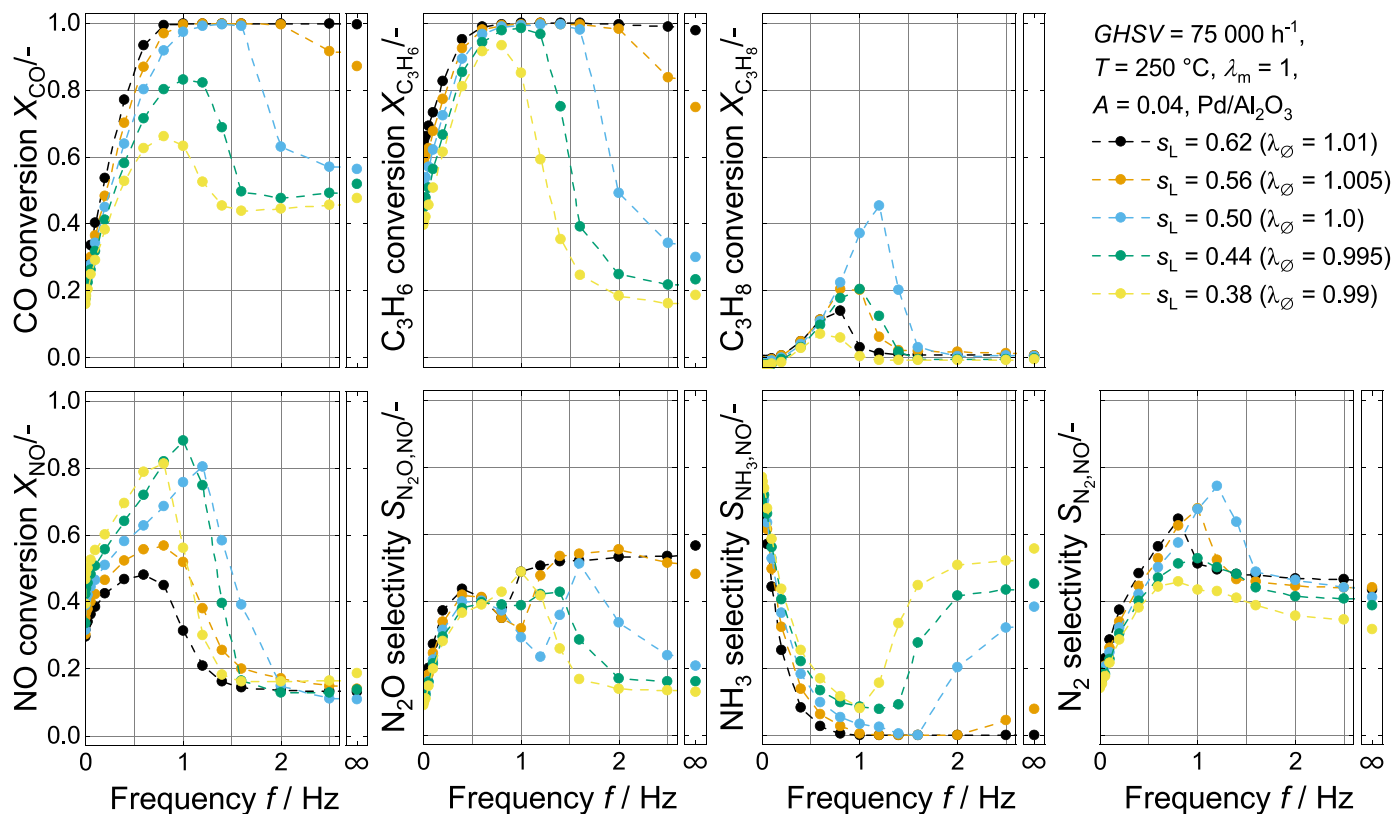


Fig. 11. Conversion of pollutants and selectivity of products formed from NO at different frequencies and split cycles at constant  $GHSV = 75\,000\text{ h}^{-1}$ ,  $T = 250\text{ °C}$ ,  $\lambda_m = 1$  and  $A = 0.04$  on Pd/Al<sub>2</sub>O<sub>3</sub>. The exhaust gas composition is listed in Table 1.

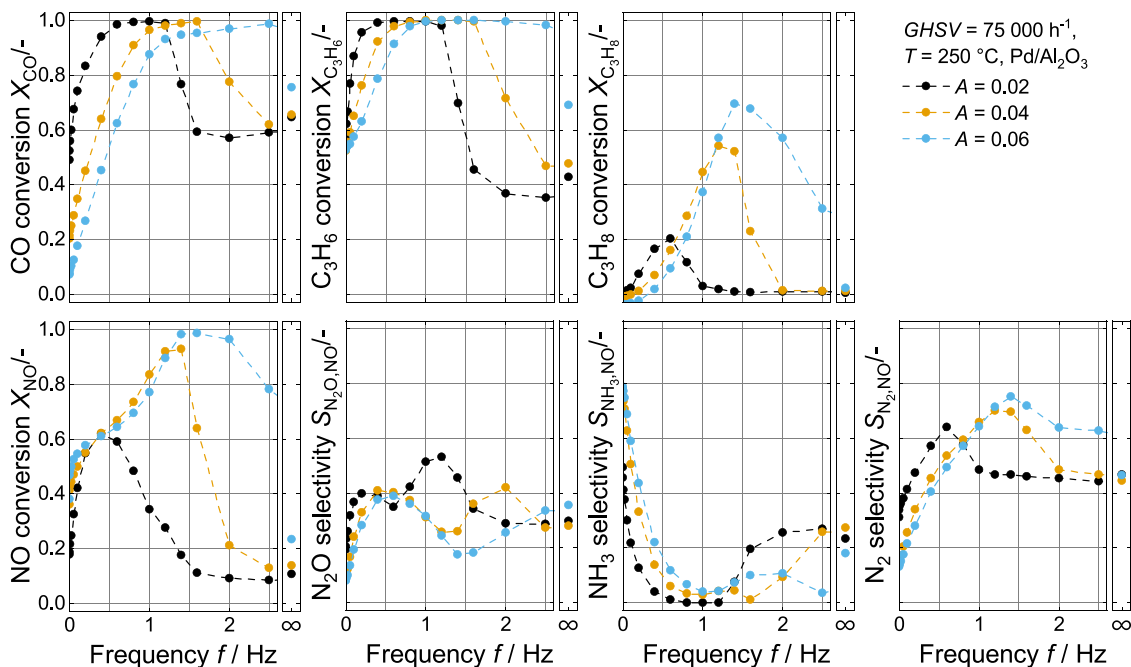


Fig. 12. Average conversion of pollutants and selectivity of products formed from NO at different frequencies and amplitude at constant  $GHSV = 75\,000\text{ h}^{-1}$ ,  $T = 250\text{ °C}$  on Pd/Al<sub>2</sub>O<sub>3</sub>. The exhaust gas composition is listed in Table 1.

temperature of 6 K and at  $100\,000\text{ h}^{-1}$  an increase in temperature of 12 K compared to the outlet temperature at  $50\,000\text{ h}^{-1}$  could be observed.

On the other hand, a strong dependence of the optimum frequency on the gas hourly space velocity can be seen during periodic operation.

The conversion maximum of the pollutants and the pattern of the product selectivities shift to higher frequencies with increasing  $GHSV$ . Notably, the increase of the optimum frequency with increasing  $GHSV$  could also be observed during rapid pulsing of reducing agents on lean NOx traps [77]. Literature suggests that higher space velocities

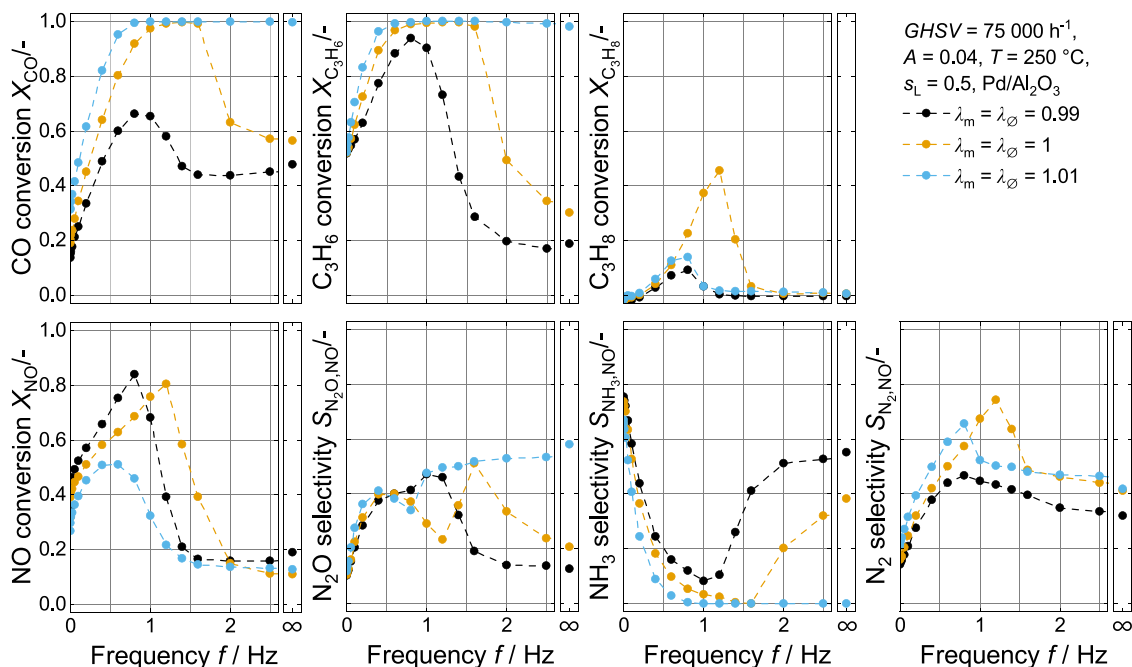


Fig. 13. Average conversion of pollutants and selectivity of products formed from NO at different frequencies and mean lambda values at constant  $GHSV = 75\,000\text{ h}^{-1}$ ,  $T = 250\text{ °C}$ ,  $s_L = 0.5$ ,  $A = 0.04$  on  $\text{Pd}/\text{Al}_2\text{O}_3$ . The exhaust gas composition is listed in Table 1.

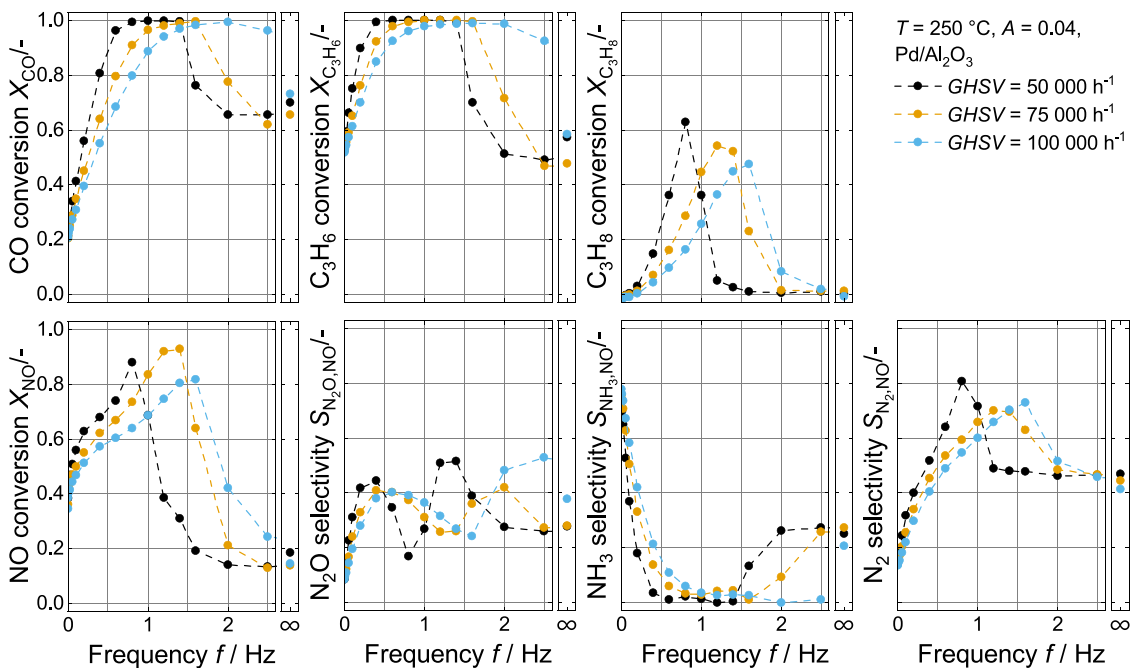


Fig. 14. Average conversion of pollutants and selectivity of products formed from NO at different frequencies and  $GHSV$  at constant  $T = 250\text{ °C}$ ,  $A = 0.04$  on  $\text{Pd}/\text{Al}_2\text{O}_3$ . The exhaust gas composition is listed in Table 1.

accelerate the saturation or depletion of adsorbents because the system is further away from the sorption equilibrium due to the shorter contact times [78,79]. The time of adsorption and desorption declines with increasing  $GHSV$  [80], thus the optimal time at each half cycle decreases and the optimal frequency increases. On the other hand, the increase of the optimal frequency with increasing  $GHSV$  can also be attributed to the reduction of back-mixing with increasing gas velocity in the plant periphery. In analogy to the behavior observed at high amplitudes (cf. Fig. 12), at the highest space velocity lower pollutant conversions can be found in the steady-state compared to  $f = 2.5\text{ Hz}$ , which is related to

insufficient back-mixing of the forced fluctuations, due to the shorter contact time of the gas phase in the reactor.

### 3.7. Influence of square wave deterioration

To investigate the influence of back-mixing behavior on the optimum frequency, the gas velocity in the tubular reactor was increased at constant  $GHSV = 50\,000\text{ h}^{-1}$  by applying a volume flow between  $3.9\text{--}7.8\text{ L}_{\text{STP}}\text{ min}^{-1}$  on monoliths with a length of  $3\text{--}6\text{ cm}$ . In comparison, in the frequency data shown above (Fig. 14) the volume flow was

varied between 3.9–7.8  $L_{STP}$  on a monolith of 3 cm length to achieve  $GHSV = 50\,000\text{--}100\,000\text{ h}^{-1}$ . Fig. 15 shows the effect of different gas velocities on the average pollutant conversion and product selectivity at  $T = 250\text{ }^\circ\text{C}$ ,  $GHSV = 50\,000\text{ h}^{-1}$  and  $A = 0.04$ . The influence of mass transport on the chemical reaction was estimated by a generalized Mears criterion [81] and can be neglected. Thus the higher velocity mainly influences the deterioration of the square wave form of the applied lean-rich cycling in the plant periphery as can be seen from the real amplitude in front of the reactor (cf. Fig. 5). Conversion of the pollutants and selectivity to the products at quasi steady-state and steady-state remain almost constant, due to the constant  $GHSV$ . Similarly, increasing the gas velocity at low frequencies does neither significantly change the conversion behavior of CO,  $C_3H_6$ ,  $C_3H_8$  and NO nor the product selectivity, which we attribute to the low relevance of back-mixing if the frequency is low. In contrast, at high frequency the deterioration of the applied square wave form increases and shifts the observed optimal frequency to lower values. Thus, the optimum frequency of the intrinsic kinetic must be much higher and is very strongly influenced by the mixing behavior upstream of the catalytic converter that is mainly caused by axial dispersion and the applied non-ideal step changes (cf. Fig. 3a). Comparing the optimal frequency of the  $C_3H_8$  conversion for the same gas velocity but different  $GHSV$  (same colors in Fig. 14 and Fig. 15), for instance, underscores that the  $GHSV$  has no significant influence on the position of optimal frequency.

### 3.8. Influence of time-on-stream (TOS)

To investigate the influence of catalyst deactivation on the optimal frequency, the catalyst was tested in a full factorial design under periodic, lean and rich operating conditions at  $T = 150\text{--}550\text{ }^\circ\text{C}$ ,  $A = 0.02\text{--}0.06$  and  $GHSV = 50\,000\text{--}100,000\text{ h}^{-1}$ . Fig. 16 shows the influence of TOS on the average pollutant conversion and product selectivities at  $GHSV = 50\,000\text{ h}^{-1}$ ,  $A = 0.04$  and  $T = 250\text{ }^\circ\text{C}$  on Pd/Al<sub>2</sub>O<sub>3</sub>. The conversion of all four pollutants and the selectivity to N<sub>2</sub> decreases with increasing TOS. The decrease in catalytic activity can be attributed to the increase in particle size of the Pd nanoparticles and the associated loss of active surface area, as can be seen from the decrease in dispersion obtained from CO chemisorption measurements of the fresh (19%) and

aged (6.5%) monolithic samples. The sintering of Pd particles has been reported in temperature regimes as also applied in the present study, namely rich conditions at temperatures of  $\geq 550\text{ }^\circ\text{C}$  [82]. Therefore, long rich phases due to low frequencies should be avoided during periodic operation of the catalyst. Interestingly, despite the increase in Pd particle size, the optimal frequency for CO,  $C_3H_6$  and  $C_3H_8$  conversion remains constant, whereas the optimal frequency for NO conversion is slightly shifted to a higher and the optimal frequencies of the secondary products are slightly shifted to lower frequencies. Possibly, the strong structural dependence of NO dissociation and recombination [60] may explain the behavior observed, as the formation of inactive nitrogen species on smaller Pd nanoparticles, with higher step/edge defect density is preferred [83].

## 4. Conclusion

In this work, a synthetic exhaust gas test bench that allows catalyst operation in highly dynamic conditions was used to investigate the influence of fast lean-rich cycling, so-called dithering, on pollutant conversion and product selectivity of Pd/Al<sub>2</sub>O<sub>3</sub> and Pd/CZ TWCs. The data obtained during dithering operation are compared with results obtained under stoichiometric steady-state conditions. Herewith, the present study aims at uncovering under which conditions periodic operation is superior to steady-state operation.

Increasing the temperature leads to a shift of the maximum conversion of the pollutant to higher frequencies in an intermediate temperature range. Thus, by controlling the optimal frequency as a function of catalyst temperature, the conversion of  $C_3H_8$  and NO can be increased by 80% at a temperature of 250 °C and a frequency of 1.2 Hz compared to stoichiometric steady-state conditions, thereby significantly improving cold start performance of the TWC. At the same time the N<sub>2</sub> selectivity could be increased by 30%.

The investigation of the split cycle and mean lambda allowed us to draw conclusions about processes taking place on the catalyst surface. In particular, it could be shown that there is an optimum time under lean and rich conditions that is directly related to the characteristic desorption time of the inhibiting surface species CO and O which occurs after the rich-lean and lean-rich switch, respectively, and determine the

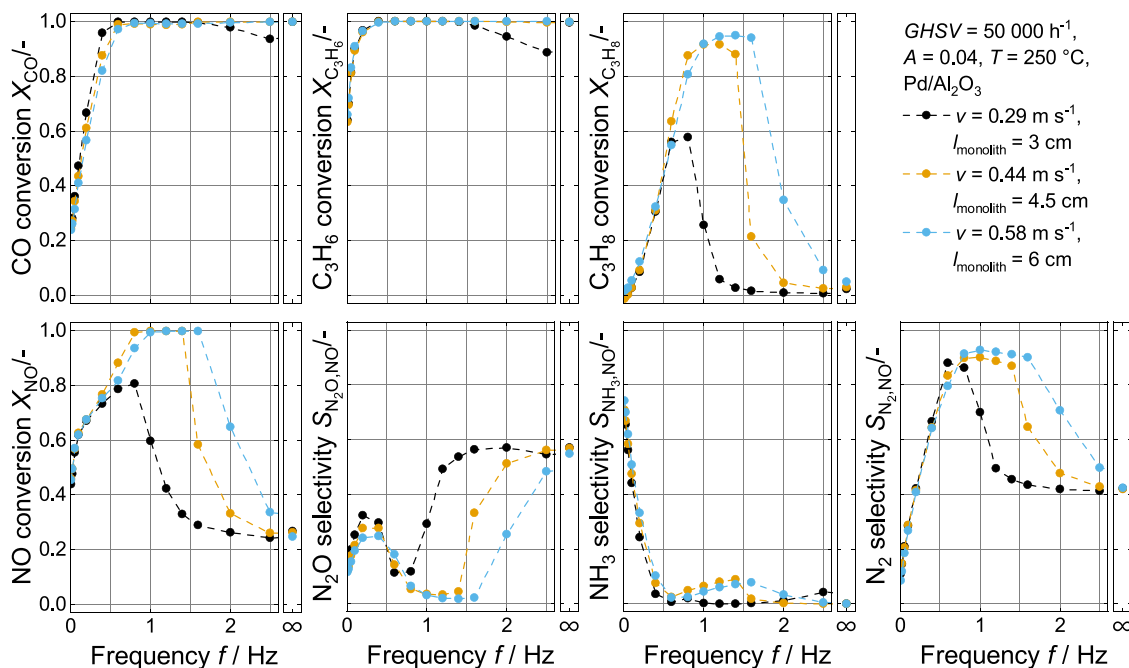
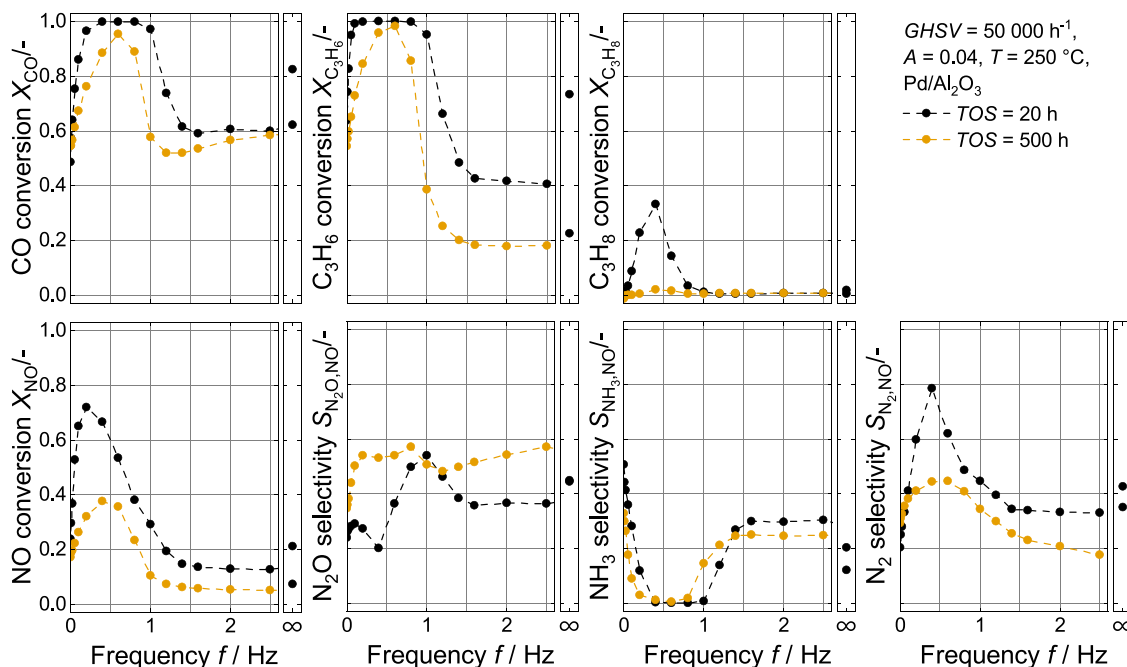


Fig. 15. Average conversion of pollutants and selectivity of products formed from NO at different frequencies and catalyst lengths at constant  $GHSV = 50\,000\text{ h}^{-1}$ ,  $T = 250\text{ }^\circ\text{C}$ ,  $A = 0.04$  on Pd/Al<sub>2</sub>O<sub>3</sub>. The exhaust gas composition is listed in Table 1.



**Fig. 16.** Average conversion of pollutants and selectivity of products formed from NO at different frequencies and time-on-stream (TOS) at constant  $GHSV = 50\,000\text{ h}^{-1}$ ,  $T = 250\text{ °C}$ ,  $A = 0.04$  on  $\text{Pd}/\text{Al}_2\text{O}_3$ . The exhaust gas composition is listed in Table 1.

optimal frequency for each pollutant. The free surface sites created in this process increase the adsorption rates of the pollutant gases and thus enable higher reaction rates for their conversion.

Through this relationship, the increase in optimal frequency with increasing amplitude can be attributed to the increase in CO and  $\text{O}_2$  partial pressure difference between lean and rich phases and the associated faster desorption time of CO and O adatoms from the catalyst surface. Since catalyst operation under optimized frequency prevents inhibition, an increase in amplitude leads to higher pollutant conversions due to the higher average CO,  $\text{H}_2$  and  $\text{O}_2$  partial pressures. The observed increase in the optimal frequency with increasing temperature can be explained by higher desorption rates and thus faster transitions between the poisoned states, i.e.  $\text{O}_2$  poisoning during lean and CO poisoning during rich phases, after a lean-rich and rich-lean switch.

In an ideal system without mixing of the lean and rich phases in front of the catalyst, the  $GHSV$  has no influence on the position of the optimum frequency. However, our results suggest that under conditions representative for real-world applications an increase of the gas velocity leads to less back-mixing upstream of the catalyst, which shifts the optimal frequency to higher values. Hence, when designing an exhaust gas aftertreatment system with forced periodic operation, close-coupled catalyst placement is desirable, as a short distance between engine and catalyst minimizes mixing of the rich and lean phases during dithering. In this regard, Pd-based catalysts as subject to this study are particularly suitable for integration close to the engine because of their high thermal stability against sintering processes. Furthermore, increasing the oxygen storage capacity of the catalyst results in lower optimal frequencies for maximum pollutant conversion at which back-mixing upstream of the catalyst is less pronounced. Nevertheless, very low frequencies should be avoided, as long rich phases accelerate sintering of the Pd nanoparticles and the resulting loss of catalytic activity surface area is typically accompanied by a drop in catalyst performance.

Since it increases the pollutant conversion at low and medium temperature, periodic operation is a highly attractive operation procedure to decrease the cold start emissions of gasoline engines equipped with a TWC for exhaust gas aftertreatment. Along with optimized and improved catalytic formulations, such advanced operation procedures will ensure compliance with increasingly stricter emission limits in the

future. Notably, the higher performance under optimized periodic operation conditions can contribute to decreasing the noble metal loading on TWC, which is of high relevance in the light of increasing scarcity and prices for noble metals such as Pd or Pt. Last but not least, the findings from this work can serve as basis for the development of a physicochemical model that aims at optimizing the temperature- and gas velocity-dependent control method of the lean-rich alternating frequency investigated by means of experiments in our present study.

#### CRediT authorship contribution statement

**Hodonj Daniel:** Conceptualization, Data curation, Formal analysis, Investigation, Methodology, Project administration, Validation, Visualization, Writing – original draft. **Borchers Michael:** Formal analysis, Investigation. **Zeh Lukas:** Formal analysis, Investigation. **Hoang Gia Trung:** Formal analysis, Investigation. **Tischer Steffen:** Supervision, Writing – review & editing. **Lott Patrick:** Conceptualization, Data curation, Project administration, Supervision, Writing – review & editing, Funding acquisition, Validation, Writing – original draft. **Deutschmann Olaf:** Project administration, Supervision, Writing – review & editing, Conceptualization, Data curation, Resources. .

#### Declaration of Competing Interest

The authors declare that they have no known competing financial interests or personal relationships that could have appeared to influence the work reported in this paper.

#### Data Availability

Data will be made available on request.

#### Acknowledgments

The authors acknowledge M. Burcea (CVT, KIT) for  $\text{N}_2$ -physisorption measurements, T. Bergfeldt (IAM, KIT) for elemental analysis, R. Popescu (LEM, KIT) for TEM measurements, K. Elfner (ITCP, KIT) for CO chemisorption measurements, and S. Lichtenberg, J. Pesek, S. Bastian

(ITCP, KIT) for their support during construction and automation of the catalyst test bench. We would like to thank Sasol and Luxfer MEL Technologies for providing alumina and ceria-zirconia support material, respectively. We thank Y. Sugaya, K. Umemoto, M. Terasawa, J. Kusaka (Waseda University, Japan), S. Tomin, Z. Yu, U. Wagner, T. Koch (IFKM, KIT), T. Mori (Toyota, Japan) and T. Mishima (Denso, Japan) for fruitful discussions in the joint FVV and AICE project “TWC-Dithering”. The German Federal Ministry for Economic Affairs and Climate Action (BMWK) is acknowledged for financial support (IGF-No. 314 EN).

## Appendix A. Supporting information

Supplementary data associated with this article can be found in the online version at doi:10.1016/j.apcatb.2023.123657.

## References

- [1] Y. Huang, N.C. Surawski, B. Organ, J.L. Zhou, O.H.H. Tang, E.F.C. Chan, Fuel consumption and emissions performance under real driving: Comparison between hybrid and conventional vehicles, *Sci. Total Environ.* 659 (2019) 275–282, <https://doi.org/10.1016/j.scitotenv.2018.12.349>.
- [2] L. Ntziachristos, G. Papadopoulos, Z. Samos, N. Tsalikidis, G. Mellios, A. Dimaratos, A. Kontses, D. Kontses, Z. Samaras, Euro 7 Impact Assessment Study, Publications Office of the European Union, Luxembourg, October 2022. doi: 10.2873/249061.
- [3] O. Deuschmann, J.-D. Grunwaldt, Exhaust gas aftertreatment in mobile systems: status, challenges, and perspectives, *Chem. Ing. Tech.* 85 (5) (2013) 595–617, <https://doi.org/10.1002/cite.201200188>.
- [4] P.L. Silveston, Automotive exhaust catalysis under periodic operation, *Catal. Today* 25 (2) (1995) 175–195, [https://doi.org/10.1016/0920-5861\(95\)00107-Q](https://doi.org/10.1016/0920-5861(95)00107-Q).
- [5] H. Muraki, H. Shinjoh, H. Sobukawa, K. Yokota, Y. Fujitani, Behavior of automotive noble metal catalysts in cycled feedstreams, *Ind. Eng. Chem. Pro. Res. Dev.* 24 (1) (1985) 43–49, <https://doi.org/10.1021/i300017a009>.
- [6] S. Tagliaferri, R. Köppel, A. Baiker, Influence of rhodium- and ceria-promotion of automotive palladium catalyst on its catalytic behaviour under steady-state and dynamic operation, *Appl. Catal. B: Environ.* 15 (3–4) (1998) 159–177, [https://doi.org/10.1016/S0926-3373\(97\)00044-1](https://doi.org/10.1016/S0926-3373(97)00044-1).
- [7] L.L. Hegedus, C.C. Chang, D.J. McEwen, E.M. Sloan, Response of catalyst surface concentrations to forced concentration oscillations in the gas phase. The NO, CO, O<sub>2</sub> System over Pt-Alumina, *Ind. Eng. Chem. Fundam.* 19 (4) (1980) 367–373, <https://doi.org/10.1021/i160076a008>.
- [8] D.J. Deka, J.A. Pihl, C.R. Thomas, W.P. Partridge, Intra-catalyst CH<sub>4</sub> oxidation pathways on a Pd/Al<sub>2</sub>O<sub>3</sub>/CeZrO<sub>x</sub>-based commercial catalyst and implications on NO<sub>x</sub> conversion profiles for a natural gas vehicle exhaust under lambda modulation, *J. Chem. Eng.* 472 (2023) 144803, <https://doi.org/10.1016/j.cej.2023.144803>.
- [9] P. Lott, M. Casapu, J.-D. Grunwaldt, O. Deuschmann, A review on exhaust gas after-treatment of lean-burn natural gas engines – From fundamentals to application, *Appl. Catal. B: Environ.* 340 (2024) 123241, <https://doi.org/10.1016/j.apcatb.2023.123241>.
- [10] H. Muraki, H. Sobukawa, Y. Fujitani, Periodic operation effects on carbon monoxide oxidation over noble metal catalysts, *Nippon Kagaku Kaishi* 2 (1985) 176–181, <https://doi.org/10.1246/nikkashi.1985.176>.
- [11] H. Shinjoh, H. Muraki, Y. Fujitani, Periodic operation effects in propane and propylene oxidation over noble metal catalysts, *Appl. Catal.* 49 (2) (1989) 195–204, [https://doi.org/10.1016/S0166-9834\(00\)83016-X](https://doi.org/10.1016/S0166-9834(00)83016-X).
- [12] H. Muraki, Y. Fujitani, NO reduction by CO over noble-metal catalysts under cycled feedstreams, *Ind. Eng. Chem. Prod. Res. Dev.* 25 (3) (1986) 414–419, <https://doi.org/10.1021/i300023a008>.
- [13] M.B. Cutlip, Concentration forcing of catalytic surface rate processes: Part I. Isothermal carbon monoxide oxidation over supported platinum, *AIChE J.* 25 (3) (1979) 502–508, <https://doi.org/10.1002/aic.690250316>.
- [14] P.-A. Carlsson, P. Thormählen, M. Skoglundh, H. Persson, E. Fridell, E. Jobson, B. Andersson, Periodic control for improved low-temperature catalytic activity, *Top. Catal.* 16 (2001) 343–347, <https://doi.org/10.1023/A:1016665216581>.
- [15] P.-A. Carlsson, S. Mollner, K. Arny, M. Skoglundh, Effect of periodic operation on the low-temperature activity for propane oxidation over Pt/Al<sub>2</sub>O<sub>3</sub> catalysts, *Chem. Eng. Sci.* 59 (20) (2004) 4313–4323, <https://doi.org/10.1016/j.ces.2004.06.024>.
- [16] D. Chan, S. Tischer, J. Heck, C. Diehm, O. Deuschmann, Correlation between catalytic activity and catalytic surface area of a Pt/Al<sub>2</sub>O<sub>3</sub> DOC: An experimental and microkinetic modeling study, *Appl. Catal. B: Environ.* 156 157 (2014) 153–165, <https://doi.org/10.1016/j.apcatb.2014.03.009>.
- [17] S. Matsumoto, H. Shinjoh, Dynamic behavior and characterization of automobile catalysts, in: G.B. Marin (Ed.), *Automotive Emission Control*, Vol. 33 of *Advances in Chemical Engineering*, Academic Press, 2007, pp. 1–46, [https://doi.org/10.1016/S0065-2377\(07\)33001-9](https://doi.org/10.1016/S0065-2377(07)33001-9).
- [18] R. Wunsch, C. Schön, M. Frey, D. Tran, S. Proskot, T. Wandrey, M. Kalogirou, J. Schäffner, Detailed experimental investigation of the NO<sub>x</sub> reaction pathways of three-way catalysts with focus on intermediate reactions of NH<sub>3</sub> and N<sub>2</sub>O, *Appl. Catal. B: Environ.* 272 (2020) 118937, <https://doi.org/10.1016/j.apcatb.2020.118937>.
- [19] T. Okajima, S. Sivakumar, H. Shingyouchi, K. Yamaguchi, J. Kusaka, M. Nagata, Modeling on a three-way catalyst used in series hybrid electric vehicles considering its specific engine operation attribute, *Ind. Eng. Chem. Res.* 60 (4) (2021) 1583–1601, <https://doi.org/10.1021/acs.iecr.0c05436>.
- [20] X. Shi, R. Seiser, J.-Y. Chen, R. Dibble, R. Cattolica, Fuel-dithering optimization of efficiency of TWC on natural gas IC engine, *SAE, Int. J. Engines* 8 (3) (2015) 1246–1252, <https://doi.org/10.4271/2015-01-1043>.
- [21] J. Braun, T. Hauber, H. Többen, J. Windmann, P. Zacke, D. Chatterjee, C. Correa, O. Deuschmann, L. Maier, S. Tischer, J. Warnatz, Three-dimensional simulation of the transient behavior of a three-way catalytic converter, *SAE Technical Paper* 2002-01-0065 (2002), <https://doi.org/10.4271/2002-01-0065>.
- [22] T. Franken, M. Roger, A.W. Petrov, A.H. Clark, M. Agote-Arán, F. Krumeich, O. Kröcher, D. Ferri, Effect of short reducing pulses on the dynamic structure, activity, and stability of Pd/Al<sub>2</sub>O<sub>3</sub> for wet lean methane oxidation, *ACS Catal.* 11 (8) (2021) 4870–4879, <https://doi.org/10.1021/acscatal.1c00328>.
- [23] D. Ferri, M. Elsener, O. Kröcher, Methane oxidation over a honeycomb Pd-only three-way catalyst under static and periodic operation, *Appl. Catal. B: Environ.* 220 (2018) 67–77, <https://doi.org/10.1016/j.apcatb.2017.07.070>.
- [24] L. Padeste, A. Baiker, Three-way catalysts in a hybrid drive system: 1. Experimental study of dynamic behavior, *Ind. Eng. Chem. Res.* 33 (5) (1994) 1113–1119, <https://doi.org/10.1021/ie00029a007>.
- [25] K.A. Karinshak, P. Lott, M.P. Harold, O. Deuschmann, In situ activation of bimetallic Pd–Pt methane oxidation catalysts, *ChemCatChem* 12 (14) (2020) 3712–3720, <https://doi.org/10.1002/cctc.202000603>.
- [26] K.G. Rappé, C. DiMaggio, J.A. Pihl, J.R. Theis, S.H. Oh, G.B. Fisher, J. Parks, V. G. Easterling, M. Yang, M.L. Stewart, K.C. Howden, Aftertreatment protocols for catalyst characterization and performance evaluation: low-temperature oxidation, storage, three-way, and NH<sub>3</sub>-SCR catalyst test protocols, *Emiss. Control Sci. Technol.* 5 (2) (2019) 183–214, <https://doi.org/10.1007/s40825-019-00120-7>.
- [27] S. Brunauer, P.H. Emmett, E. Teller, Adsorption of gases in multimolecular layers, *J. Am. Chem. Soc.* 60 (2) (1938) 309–319, <https://doi.org/10.1021/ja01269a023>.
- [28] J. Schindelin, I. Arganda-Carreras, E. Frise, V. Kaynig, M. Longair, T. Pietzsch, S. Preibisch, C. Rueden, S. Saalfeld, B. Schmid, J.-Y. Tinevez, D.J. White, V. Hartenstein, K. Eliceiri, P. Tomancak, A. Cardona, Fiji: an open-source platform for biological-image analysis, *Nat. Methods* 9 (7) (2012) 676–682, <https://doi.org/10.1038/NMETH.2019>.
- [29] C. Karakaya, O. Deuschmann, A simple method for CO chemisorption studies under continuous flow: Adsorption and desorption behavior of Pt/Al<sub>2</sub>O<sub>3</sub> catalysts, *Appl. Catal. A: Gen.* 445–446 (2012) 221–230, <https://doi.org/10.1016/j.apcata.2012.08.022>.
- [30] G. Bergeret, P. Gallezot, Particle size and dispersion measurements, vol. 7, in: G. Ertl, H. Knözinger, F. Schüth, J. Weitkamp (Eds.), *Handbook of Heterogeneous Catalysis*, Wiley-VCH Verlag GmbH & Co. KGaA, Weinheim, 2008, pp. 738–765, <https://doi.org/10.1002/9783527610044.hetcat0038>, vol. 7.
- [31] R.H. Hammerle, C.H. Wu, Effect of High Temperatures on Three-Way Automotive Catalysts, *SAE Technical Paper* 1984-02-01 (1984), doi:10.4271/840549.
- [32] P.L. Silveston, Automotive exhaust catalysis: is periodic operation beneficial? *Chem. Eng. Sci.* 51 (10) (1996) 2419–2426, [https://doi.org/10.1016/0009-2509\(96\)00098-X](https://doi.org/10.1016/0009-2509(96)00098-X).
- [33] J. Kašpar, P. Fornasiero, N. Hickey, Automotive catalytic converters: current status and some perspectives, *Catal. Today* 77 (4) (2003) 419–449, [https://doi.org/10.1016/S0920-5861\(02\)00384-X](https://doi.org/10.1016/S0920-5861(02)00384-X).
- [34] J.C. Summers, L.L. Hegedus, Modes of catalyst deactivation in stoichiometric automobile exhaust, *Ind. Eng. Chem. Prod. Res. Dev.* 18 (4) (1979) 318–324, <https://doi.org/10.1021/i360072a018>.
- [35] K. Yokota, H. Muraki, Y. Fujitani, Rh-Free Three-Way Catalysts for Automotive Exhaust Control, *SAE Technical Paper* 1985-02-01 (1985), doi:10.4271/850129.
- [36] M. Weilenmann, Aspects of highly transient catalyst simulation, *Catal. Today* 188 (1) (2012) 121–134, <https://doi.org/10.1016/j.cattod.2011.10.002>.
- [37] M. Roger, O. Kröcher, D. Ferri, Assessing the effect of O<sub>2</sub> dithering on CH<sub>4</sub> oxidation on Pd/Al<sub>2</sub>O<sub>3</sub>, *Chem. Eng. J.* 451 (2023) 138865, <https://doi.org/10.1016/j.cej.2022.138865>.
- [38] D. Meyer, J. Friedland, J. Schumacher, R. Güttel, The periodic transient kinetics method for investigation of kinetic process dynamics under realistic conditions: Methanation as an example, *Chem. Eng. Res. Des.* 173 (2021) 253–266, <https://doi.org/10.1016/j.cherd.2021.07.011>.
- [39] W.B. Bae, D.Y. Kim, S.W. Byun, M. Hazlett, D.Y. Yoon, C. Jung, C.H. Kim, S. B. Kang, Emission of NH<sub>3</sub> and N<sub>2</sub>O during NO reduction over commercial aged three-way catalyst (TWC): Role of individual reductants in simulated exhausts, *Chem. Eng. J. Adv.* 9 (2022) 100222, <https://doi.org/10.1016/j.cej.2021.100222>.
- [40] R. Burch, D.J. Crittle, M.J. Hayes, C–H bond activation in hydrocarbon oxidation on heterogeneous catalysts, *Catal. Today* 47 (1–4) (1999) 229–234, [https://doi.org/10.1016/S0920-5861\(98\)00303-4](https://doi.org/10.1016/S0920-5861(98)00303-4).
- [41] P. Lott, S. Bastian, H. Többen, L. Zimmermann, O. Deuschmann, Formation of nitrous oxide over Pt-Pd oxidation catalysts: Secondary emissions by interaction of hydrocarbons and nitric oxide, *Appl. Catal. A: Gen.* 651 (2023) 119028, <https://doi.org/10.1016/j.apcata.2023.119028>.
- [42] O. Deuschmann, R. Schmidt, F. Behrendt, J. Warnatz, Numerical modeling of catalytic ignition, *Symp. (Int.) Combust.* 26 (1) (1996) 1747–1754, [https://doi.org/10.1016/S0082-0784\(96\)80400-0](https://doi.org/10.1016/S0082-0784(96)80400-0).
- [43] J. Koop, O. Deuschmann, Detailed surface reaction mechanism for Pt-catalyzed abatement of automotive exhaust gases, *Appl. Catal. B: Environ.* 91 (1–2) (2009) 47–58, <https://doi.org/10.1016/j.apcatb.2009.05.006>.

- [44] P.L. Silveston, R.R. Hudgins, Combustion systems, in: P. Silveston, R. Hudgins (Eds.), *Periodic Operation of Chemical Reactors*, Butterworth-Heinemann, Oxford, 2013, pp. 123–140, <https://doi.org/10.1016/B978-0-12-391854-3.00005-X>.
- [45] Y. Barshad, E. Gulari, A novel catalytic reactor system for transient response and its use in CO oxidation on Pd/Al<sub>2</sub>O<sub>3</sub>, *J. Catal.* 94 (2) (1985) 468–477, [https://doi.org/10.1016/0021-9517\(85\)90211-8](https://doi.org/10.1016/0021-9517(85)90211-8).
- [46] X. Zhou, Y. Barshad, E. Gulari, CO oxidation on Pd/Al<sub>2</sub>O<sub>3</sub>. Transient response and rate enhancement through forced concentration cycling, *Chem. Eng. Sci.* 41 (5) (1986) 1277–1284, [https://doi.org/10.1016/0009-2509\(86\)87100-7](https://doi.org/10.1016/0009-2509(86)87100-7).
- [47] A. Jaree, R.R. Hudgins, H.M. Budman, P.L. Silveston, V.Z. Yakhnin, M. Menzinger, Hysteresis and extinction waves in catalytic CO oxidation caused by reactant concentration perturbations in a packed-bed reactor, *Ind. Eng. Chem. Res.* 42 (8) (2003) 1662–1673, <https://doi.org/10.1021/i00012a010>.
- [48] B.K. Cho, Dynamic behavior of a single catalyst pellet 1. Symmetric concentration cycling during CO oxidation over Pt/Al<sub>2</sub>O<sub>3</sub>, *Ind. Eng. Chem. Fundam.* 22 (4) (1983) 410–420, <https://doi.org/10.1021/i100012a010>.
- [49] I. Mejía-Centeno, S. Castillo, G.A. Fuentes, Enhanced emissions of NH<sub>3</sub>, N<sub>2</sub>O and H<sub>2</sub> from a Pd-only TWC and supported Pd model catalysts: Light-off and sulfur level studies, *Appl. Catal. B: Environ.* 119–120 (2012) 234–240, <https://doi.org/10.1016/j.apcatb.2012.02.030>.
- [50] F. Dhainaut, S. Pietrzyk, P. Granger, NO + H<sub>2</sub> reaction on Pd/Al<sub>2</sub>O<sub>3</sub> under lean conditions: kinetic study, *Top. Catal.* 42 (2007) 135–141, <https://doi.org/10.1007/s11244-007-0166-2>.
- [51] S.A. Malamis, M. Li, W.S. Epling, M.P. Harold, Steady state and lean-rich cycling study of a three-way NO<sub>x</sub> storage catalyst: Experiments, *Appl. Catal. B: Environ.* 237 (2018) 588–602, <https://doi.org/10.1016/j.apcatb.2018.06.001>.
- [52] M. Shen, M. Yang, J. Wang, J. Wen, M. Zhao, W. Wang, Pd/Support interface-promoted Pd–Ce<sub>0.7</sub>Zr<sub>0.3</sub>O<sub>2</sub>–Al<sub>2</sub>O<sub>3</sub> automobile three-way catalysts: studying the dynamic oxygen storage capacity and CO, C<sub>3</sub>H<sub>8</sub>, and NO conversion, *J. Phys. Chem. C* 113 (8) (2009) 3212–3221, <https://doi.org/10.1021/jp805128u>.
- [53] A. Satsuma, M. Yanagihara, J. Ohyama, K. Shimizu, Oxidation of CO over Ru/Ceria prepared by self-dispersion of Ru metal powder into nano-sized particle, *Catal. Today* 201 (2013) 62–67, <https://doi.org/10.1016/j.cattod.2012.03.048>.
- [54] A.M. Gänzler, M. Casapu, P. Vernoux, S. Lorient, F.J. Cadete Santos Aires, T. Epicier, B. Betz, R. Hoyer, J.-D. Grunwaldt, Tuning the structure of platinum particles on ceria in situ for enhancing the catalytic performance of exhaust gas catalysts, *Angew. Chem., Int. Ed.* 56 (42) (2017) 13078–13082, <https://doi.org/10.1002/anie.201707842>.
- [55] Y. An, S.-Y. Chen, B. Wang, L. Zhou, G. Hao, Y. Wang, J. Chen, C.-K. Tsung, Z. Liu, L.-Y. Chou, Controlling the metal–support interaction with steam-modified ceria to boost Pd activity towards low-temperature CO oxidation, *J. Mater. Chem. A* 11 (31) (2023) 16838–16845, <https://doi.org/10.1039/D3TA02626D>.
- [56] H.-W. Jen, G. Graham, W. Chun, R. McCabe, J.-P. Cuif, S. Deutsch, O. Touret, Characterization of model automotive exhaust catalysts: Pd on ceria and ceria-zirconia supports, *Catal. Today* 50 (2) (1999) 309–328, [https://doi.org/10.1016/S0920-5861\(98\)00512-4](https://doi.org/10.1016/S0920-5861(98)00512-4).
- [57] E. Ogel, M. Casapu, D.E. Doronkin, R. Popescu, H. Störmer, C. Mechler, G. Marzun, S. Barcikowski, M. Türk, J.-D. Grunwaldt, Impact of preparation method and hydrothermal aging on particle size distribution of Pt/γ-Al<sub>2</sub>O<sub>3</sub> and its performance in CO and NO oxidation, *J. Phys. Chem. C* 123 (9) (2019) 5433–5446, <https://doi.org/10.1021/acs.jpcc.8b11065>.
- [58] J. Schütz, H. Störmer, P. Lott, O. Deutschmann, Effects of hydrothermal aging on CO and NO oxidation activity over monometallic and bimetallic Pt-Pd catalysts, *Catalysts* 11 (3) (2021) 300, <https://doi.org/10.3390/catal11030300>.
- [59] J. Kašpar, P. Fornasiero, M. Graziani, Use of CeO<sub>2</sub>-based oxides in the three-way catalysis, *Catal. Today* 50 (2) (1999) 285–298, [https://doi.org/10.1016/S0920-5861\(98\)00510-0](https://doi.org/10.1016/S0920-5861(98)00510-0).
- [60] A. Iglesias-Juez, A. Martínez-Arias, M. Fernández-García, Metal–promoter interface in Pd/(Ce,Zr)O<sub>x</sub>/Al<sub>2</sub>O<sub>3</sub> catalysts: effect of thermal aging, *J. Catal.* 221 (1) (2004) 148–161, <https://doi.org/10.1016/j.jcat.2003.07.010>.
- [61] Y. Yamakawa, R. Inoue, Y. Kubo, K. Yamaguchi, J. Kusaka, Conversion performance prediction of thermal-deteriorated three-way catalysts: surface reaction model development considering platinum group metals and co-catalyst, *SAE Technical Paper* (2021), <https://doi.org/10.4271/2021-24-0077>, 2021-24-00777.
- [62] S. Hilaire, X. Wang, T. Luo, R. Gorte, J. Wagner, A comparative study of water-gas-shift reaction over ceria supported metallic catalysts, *Appl. Catal. A: Gen.* 215 (1–2) (2001) 271–278, [https://doi.org/10.1016/S0926-860X\(01\)00535-X](https://doi.org/10.1016/S0926-860X(01)00535-X).
- [63] S. Pares-Esclapez, M.J. Illán-Gómez, C.S.-M. de Lecea, A. Bueno-López, On the importance of the catalyst redox properties in the N<sub>2</sub>O decomposition over alumina and ceria supported Rh, Pd and Pt, *Appl. Catal. B: Environ.* 96 (3–4) (2010) 370–378, <https://doi.org/10.1016/j.apcatb.2010.02.034>.
- [64] T. Nakase, T. Hattori, J. Naito, K. Kondo, Method of operating a three-way catalyst for internal combustion, Patent No. US4199938A (1980).
- [65] J. Rink, N. Meister, F. Herbst, M. Votsmeier, Oxygen storage in three-way-catalysts is an equilibrium controlled process: Experimental investigation of the redox thermodynamics, *Appl. Catal. B: Environ.* 206 (2017) 104–114, <https://doi.org/10.1016/j.apcatb.2016.12.052>.
- [66] G. Keitl, J. Rink, F. Wen, L. Jongen, A. Hofmann, M. Votsmeier, A. Terfort, J. Gieshoff, Impact of test conditions on the oxygen storage capacity of Pd loaded cerium zirconium oxide, *Top. Catal.* 60 (3–5) (2017) 272–277, <https://doi.org/10.1007/s11244-016-0611-1>.
- [67] J. Zhu, M. Shen, J. Wang, X. Wang, J. Wang, N<sub>2</sub>O formation during NO<sub>x</sub> storage and reduction using C<sub>3</sub>H<sub>6</sub> as reductant, *Catal. Today* 297 (2017) 92–103, <https://doi.org/10.1016/j.cattod.2016.11.035>.
- [68] Y. Barshad, E. Gulari, A dynamic study of CO oxidation on supported platinum, *AIChE J.* 31 (4) (1985) 649–658, <https://doi.org/10.1002/aic.690310415>.
- [69] B. Banse, D.T. Wickham, B.E. Koel, Transient kinetic studies of the catalytic reduction of NO by CO on platinum, *J. Catal.* 119 (1) (1989) 238–248, [https://doi.org/10.1016/0021-9517\(89\)90149-8](https://doi.org/10.1016/0021-9517(89)90149-8).
- [70] A. Reihani, B. Patterson, J.W. Hoard, G.B. Fisher, Global kinetic modeling of rapidly pulsed reductants for lean NO<sub>x</sub> traps: frequency domain analysis and impact of mass transfer, *Appl. Catal. B: Environ.* 254 (2019) 223–236, <https://doi.org/10.1016/j.apcatb.2019.04.076>.
- [71] T. Engel, G. Ertl, Elementary steps in the catalytic oxidation of carbon monoxide on platinum metals, *Adv. Catal.* 28 (1979) 1–78, [https://doi.org/10.1016/S0360-0564\(08\)60133-9](https://doi.org/10.1016/S0360-0564(08)60133-9).
- [72] B. Shan, L. Wang, J. Hyun, Y. Sang, Y. Zhao, J.B. Nicholas, Dissociative adsorption of O<sub>2</sub> on clean and CO-precovered Pt surfaces, *MRS Proc.* 1084 (2008), <https://doi.org/10.1557/PROC-1084-S05-01>.
- [73] J.H. Miners, A.M. Bradshaw, P. Gardner, Direct observation of surface isocyanate (NCO) formation during the CO+NO reaction on Pt100, *Phys. Chem. Chem. Phys.* 1 (20) (1999) 4909–4912, <https://doi.org/10.1039/A905548G>.
- [74] N. Macleod, R.M. Lambert, An in situ DRIFTS study of efficient lean NO<sub>x</sub> reduction with H<sub>2</sub> + CO over Pd/Al<sub>2</sub>O<sub>3</sub>: the key role of transient NCO formation in the subsequent generation of ammonia, *Appl. Catal. B: Environ.* 46 (3) (2003) 483–495, [https://doi.org/10.1016/S0926-3373\(03\)00289-3](https://doi.org/10.1016/S0926-3373(03)00289-3).
- [75] S.B. Kang, K. Karinshak, P.W. Chen, S. Golden, M.P. Harold, Coupled methane and NO<sub>x</sub> conversion on Pt + Pd/Al<sub>2</sub>O<sub>3</sub> monolith: Conversion enhancement through feed modulation and Mn<sub>0.5</sub>Fe<sub>2.5</sub>O<sub>4</sub> spinel addition, *Catal. Today* 360 (2021) 284–293, <https://doi.org/10.1016/j.cattod.2020.02.039>.
- [76] K. Karinshak, P.W. Chen, R.-F. Liu, S.J. Golden, M.P. Harold, Optimizing feed modulation for coupled methane and NO<sub>x</sub> conversion over Pd-Pt/Mn<sub>0.5</sub>Fe<sub>2.5</sub>O<sub>4</sub>/Al<sub>2</sub>O<sub>3</sub> monolith catalyst, *Appl. Catal. B: Environ.* 304 (2022) 120607, <https://doi.org/10.1016/j.apcatb.2021.120607>.
- [77] A. Reihani, G.B. Fisher, J.W. Hoard, J.R. Theis, J.D. Pakko, C.K. Lambert, Rapidly pulsed reductants for diesel NO<sub>x</sub> reduction with lean NO<sub>x</sub> traps: effects of pulsing parameters on performance, *Appl. Catal. B: Environ.* 223 (2018) 177–191, <https://doi.org/10.1016/j.apcatb.2017.07.054>.
- [78] H. Patel, Fixed-bed column adsorption study: a comprehensive review, *Appl. Water Sci.* 9 (3) (2019), <https://doi.org/10.1007/s13201-019-0927-7>.
- [79] L. Sheng, Y. Zhang, F. Tang, S. Liu, Mesoporous/microporous silica materials: preparation from natural sands and highly efficient fixed-bed adsorption of methylene blue in wastewater, *Microporous Mesoporous Mater.* 257 (2018) 9–18, <https://doi.org/10.1016/j.micromeso.2017.08.023>.
- [80] V. Recupero, L. Pino, M. Cordaro, A. Vita, F. Cipiti, M. Laganà, CO clean-up transient device integrated to a preferential oxidation reactor for PEFC electric vehicles, *Fuel Process. Technol.* 85 (13) (2004) 1445–1452, <https://doi.org/10.1016/j.fuproc.2003.10.001>.
- [81] O. Görke, P. Pfeifer, K. Schubert, Kinetic study of ethanol reforming in a microreactor, *Appl. Catal. A: Gen.* 360 (2) (2009) 232–241, <https://doi.org/10.1016/j.apcata.2009.03.026>.
- [82] X. Chen, Y. Cheng, C.Y. Seo, J.W. Schwank, R.W. McCabe, Aging, re-dispersion, and catalytic oxidation characteristics of model Pd/Al<sub>2</sub>O<sub>3</sub> automotive three-way catalysts, *Appl. Catal. B: Environ.* 163 (2015) 499–509, <https://doi.org/10.1016/j.apcatb.2014.08.018>.
- [83] D.R. Rainer, M. Koranne, S.M. Vesecky, D.W. Goodman, CO + O<sub>2</sub> and CO + NO reactions over Pd/Al<sub>2</sub>O<sub>3</sub> catalysts, *J. Phys. Chem. B* 101 (50) (1997) 10769–10774, <https://doi.org/10.1021/jp971262z>.